UNIVERSITY OF HELSINKI REPORT SERIES IN PHYSICS

HU-P-D230

OPTIMIZING COMPUTER TOMOGRAPHY EXAMINATIONS BY USING ANTHROPOMORPHIC PHANTOMS AND MOSFET DOSIMETERS

Touko Kaasalainen

Department of Physics
Faculty of Science
University of Helsinki
Helsinki, Finland

HUS Medical Imaging Center
Helsinki University Hospital
Helsinki, Finland

ACADEMIC DISSERTATION

To be presented, with the permission of the Faculty of Science of the University of Helsinki, for public examination in the Linus Torvalds Auditorium B123 (Exactum, Gustaf Hällströmin katu 2B, Helsinki, Finland) on 25 September 2015 at 12 o´clock noon.

Helsinki, 2015

Supervising professor

Professor Sauli Savolainen, Ph.D.
Department of Physics
University of Helsinki, Finland

HUS Medical Imaging Center
University of Helsinki and Helsinki University Hospital, Finland

Supervisor:

Docent Mika Kortesniemi, Ph.D.
HUS Medical Imaging Center
University of Helsinki and Helsinki University Hospital, Finland

Reviewers:

Docent Mika Kapanen, Ph.D.
Department of Oncology
Tampere University Hospital, Finland

Docent Juha Nikkinen, Ph.D.
Department of Oncology and Radiotherapy
Oulu University Hospital, Finland

Opponent:

Professor Miika Nieminen, Ph.D.
Department of Radiology
University of Oulu and Oulu University Hospital, Finland

ISSN 0356-0961
ISBN 978-951-51-0593-6 (pbk)
ISBN 978-951-51-0594-3 (pdf version)

Helsinki University Print (Unigrafia Oy)
Helsinki, 2015

T. Kaasalainen: Optimizing computer tomography examinations by using anthropomorphic phantoms and MOSFET dosimeters, University of Helsinki, 2015, 63 pp. + appendices, University of Helsinki, Report Series in Physics, HU-P-D230, ISSN 0356-0961, ISBN 978-951-51-0593-6 (pbk), ISBN 978-951-51-0594-3 (pdf version)

Keywords: medical physics, computer tomography, radiation protection, anthropomorphic phantom, MOSFET

Classification (INSPEC): A8760M, A8770E, B7510P, B7530B, B2560R

ABSTRACT

The number of computed tomography (CT) examinations has increased in recent years due to developments in scanner technology and the increased diagnostic capabilities of CT. Nowadays, CT has become a major contributor to accumulated radiation doses from radiological examinations, accounting for approximately 60% of the overall medical radiation dose in Western countries. Ionizing radiation is generally considered harmful to health, and current knowledge suggests that the risk for stochastic effects increases linearly with radiation dose. Minimizing patient doses in CT requires effective optimization practices, including both technical and clinical approaches. CT optimization aims to reduce patients' exposure to radiation without compromising image quality for diagnosis.

The aim of this dissertation was to explore the feasibility of using anthropomorphic phantoms and metal-oxide-semiconductor field-effect transistors (MOSFETs) in CT optimization and patient dose measurements, and to study CT optimization in versatile clinical situations. Specifically, this thesis focused on studying the effects of patient centering on the CT scanner isocenter by determining changes in patient dose and image quality. Additionally, as a part of this thesis, we constructed and optimized ultralow-dose CT protocols for craniosynostosis imaging, and explored different optimization methods for reducing radiation exposure to eye lenses. Moreover, fetal radiation doses were assessed in the most typical CT examinations of a pregnant woman which also place the fetus at the highest risk for ionizing radiation-induced health detriments.

Anthropomorphic phantoms and MOSFET dosimeters proved feasible in CT optimization even with the use of ultralow-dose levels. Patient vertical off-centering posed a common and serious problem in chest CT, as a majority of the scanned patients were positioned below the isocenter of the CT scanner,

which significantly affected both radiation dose and image quality. This exposes the radiosensitive anterior surface tissues, including the breasts and thyroid gland, to greater risk. Special attention should focus on pediatric patients in particular, as they were typically miscentered lower than adults were.

The use of constructed ultralow-dose CT protocols with model-based iterative reconstruction can enable craniosynostosis CT imaging with sufficient image quality for diagnosis with an effective dose of less than 20 µSv for the patient. This dose level was approximately 85% lower than the level used in routine CT protocols in the hospital for craniosynostosis, and was comparable to the radiation exposure of a plain-skull radiography examination.

The most efficient method for reducing the dose to the eye lens proved to be gantry tilting, which leaves the eye lenses outside the primary radiation beam, thereby reducing the absorbed dose up to 75%. However, measurements with two different anthropomorphic head phantoms showed that patient geometry significantly affects dose-reduction capabilities. If lenses can only partially be cropped outside the primary beam, organ-based tube current modulation or bismuth shields may also be used for reducing the dose to the lenses.

Based on the measured absorbed doses in this thesis, the radiation dose to the fetus poses no obstacle to an optimized CT examination with a medically necessary indication. The volumetric CT dose index ($CTDI_{vol}$) provides a rough estimate of the fetal dose when the uterus is in the primary radiation beam, although the extent of the scan range has a substantial effect on the fetal dose. The results support the conception that when the fetus or uterus is not in the scan range, the fetal dose is affected mainly by the distance from the scan range.

TIIVISTELMÄ

Tietokonetomografiatutkimusten (TT) määrä on kasvanut laitekehityksen sekä TT:n lisääntyneiden diagnostisten sovelluskohteiden ansiosta viime vuosien aikana huomattavasti. Siitä on nykyisellään tullut länsimaissa radiologisista menetelmistä eniten kollektiivista sädeannosta kerryttävä menetelmä noin 60 %:n osuudella kaikkien lääketieteellisten röntgentutkimusten aiheuttamasta yhteisestä kokonaisannoksesta. Ionisoivaa säteilyä pidetään yleisesti ottaen terveydelle haitallisena, ja nykytietämyksen mukaan säteilyn tilastollisten haittavaikutusten riski kasvaa lineaarisesti säteilyannoksen kasvaessa. Jotta potilaiden saamaa säteilyaltistusta voitaisiin TT:ssä vähentää, on tehokkaiden optimointimenetelmien, niin teknisten kuin myös kliinisten, käyttö tarpeen. TT-optimoinnin tarkoituksena on vähentää potilaiden saamia säteilyannoksia ilman että diagnostinen kuvanlaatu oleellisesti kärsii.

Tämän työn tarkoituksena oli tutkia ihmisenkaltaisten potilasvasteiden (l. antropomorfisten fantomien) ja puolijohdetekniikkaan perustuvien MOSFET-dosimetrien soveltuvuutta TT-optimointiin sekä tutkia TT-optimointia useissa kliinisissä sovelluksissa. Työssä tutkittiin erityisesti potilaan vertikaalisuunnan keskittämisen vaikutuksia potilasannosten sekä kuvanlaadun osalta. Lisäksi tämän väitöskirjan osana luotiin kraniosynostoosipotilaiden kuvantamista varten erittäin matalaa annostasoa hyödyntävät TT-protokollat sekä tutkittiin erilaisten optimointimenetelmien käyttöä silmän linssien säteilyaltistuksen pienentämiseksi. Työssä määritettiin myös sikiön saamia säteilyannoksia yleisimmissä TT-tutkimuksissa, joita raskaana olevalle naiselle mahdollisesti joudutaan tekemään, ja jotka aiheuttavat sikiölle merkittävimmän ionisoivasta säteilystä peräisin olevan terveysriskin.

Antropomorfiset fantomit ja MOSFET-dosimetrit osoittautuivat TT-tutkimusten optimointiin soveltuviksi jopa erittäin matalilla annostasoilla. Potilaan vertikaalinen keskitysvirhe havaittiin olevan vakava ja yleinen ongelma keuhkojen TT-tutkimuksissa, sillä suurin osa kliinisistä potilaista keskitettiin TT-laitteen isosentriin nähden liian alas, vaikuttaen huomattavasti sekä säteilyannoksiin että kuvanlaatuun. Tämä altistaa erityisesti säteilyherkät anterioriset pintakudokset, kuten rinnat ja kilpirauhasen, suuremmalle riskille. Erityisesti lasten kohdalla huolelliseen keskittämiseen tulisi kiinnittää huomiota, sillä keskitysvirhe oli lapsipotilailla aikuisia suurempi.

Kraniosynostoosipotilaiden TT-tutkimus voitiin tehdä työssä kehitetyllä mallipohjaista iteratiivista rekonstruktiota hyödyntävällä erittäin matalan annostason omaavalla TT-protokollalla jopa alle 20 µSv efektiivisellä annoksella potilaalle ilman että diagnostiikkaan tarvittava kuvanlaatu oleellisesti kärsi. Tämä oli noin 85 % vähemmän kuin sairaalassa rutiinisti

käytettävä TT-protokolla kraniosynostoosipotilaiden kuvaukseen tuottaa, vastaten samalla myös tavallisen kalloröntgenkuvan tuottamaa annostasoa.

TT-gantryn kippaus siten, että silmän linssit jäävät primäärisäteilykeilan ulkopuolelle, osoittautui tehokkaimmaksi menetelmäksi pienennettäessä silmän linssien annostasoa tavallisissa pään TT-tutkimuksissa. Näin saavutettiin jopa 75 %:n annossäästö verrattuna protokollaan, jossa ei käytetty erillisiä optimointimenetelmiä. Mittaukset kahdella pääfantomilla kuitenkin osoittivat pään geometrian vaikuttavan huomattavasti annosoptimointiin. Kuvauksissa, joissa silmän linssit voidaan jättää vain osittain primäärikeilan ulkopuolelle, voidaan käyttää silmän linssien suojaamiseen myös joko elinkohtaista putkivirran modulaatiota tai vismuttisuojia.

Sikiön saamat säteilyannokset eivät ole tässä työssä määritettyjen absorboituneiden annosten perusteella este optimoidulle TT-tutkimukselle lääketieteellisen indikaation niin vaatiessa. TT-annosten tilavuuskeskiarvoa ($CTDI_{vol}$) voidaan pitää sikiöannokselle karkeana arviona kohdun ollessa primäärisäteilykeilassa, joskin kuvausalueen laajuudella on huomattava vaikutus sikiön saamaan säteilyannokseen. Saadut tulokset tukevat myös käsitystä, että sikiön tai kohdun ollessa kuvausalueen ulkopuolella, sikiöannos riippuu pääosin sikiön etäisyydestä kuvausalueelta.

PREFACE

The main work for this thesis took place during the years 2011 and 2015 at the HUS Medical Imaging Center, Helsinki University Hospital. I therefore owe my gratitude to both the Managing and Deputy Managing Directors of the HUS Medical Imaging Center, Jyrki Putkonen and Pekka Tervahartiala, for providing me with excellent research facilities at the hospital. Furthermore, I warmly acknowledge both the current and former Heads of the Department of Physics, Professors Hannu Koskinen and Juhani Keinonen, for supporting my studies at the University of Helsinki.

I am most grateful to my supervisor, Docent Mika Kortesniemi, Chief Physicist of the HUS Medical Imaging Center, for his great support and guidance during all the stages of this work. Our enlightening discussions on the research topics or anything else were deeply rewarding. I'm also grateful to Professor Sauli Savolainen, Chief Physicist of the HUS Medical Imaging Center, for his aid and guidance in both conducting research and working at the hospital. He has been an excellent, supportive boss, and his enthusiastic attitude has encouraged me to continue in the field of research.

I also thank the official reviewers of this thesis, Docents Mika Kapanen and Juha Nikkinen, for their constructive remarks and criticism, and Stephen Stalter, for revising the language of the thesis.

I also offer my sincere gratitude to my co-authors, physicists Kirsi Palmu, Vappu Reijonen, Anniina Lampinen, Anna Kelaranta and Paula Toroi, medical doctors Junnu Leikola, Riku Kivisaari and Raija Seuri, radiographer Ulla Nikupaavo, and postdoctoral researcher in Health Science Sanna-Mari Ahonen, who have supported and participated in this research. Without their output, completing this thesis would have been impossible. Further, I want to thank the Radiological Society of Finland for the grant to finish the manuscript.

I further thank all my colleagues and workmates at the hospital for their help and advice over the years. It has been a pleasure working with you all.

I also want to say 'Obrigado por tudo, minha querida' to Stefanie Szabo, who enabled and supported me to finish the manuscript under the palm trees and sun in wonderful and exotic Brazil. Finally, and most importantly, I extend my greatest appreciation to my parents, Auli and Matti Kaasalainen, and to my siblings for their enormous support and care throughout my life.

Helsinki, August 2015
Touko Kaasalainen

CONTENTS

LIST OF ORIGINAL PUBLICATIONS

This thesis was based on five original articles, referred to in the text by their Roman numerals.

I Kaasalainen T, Palmu K, Lampinen A, Kortesniemi M. Effect of vertical positioning on organ dose, image noise and contrast in pediatric chest CT – phantom study. Pediatr Radiol 2013;43:673-684.

II Kaasalainen T, Palmu K, Reijonen V, Kortesniemi M. Effect of patient centering on patient dose and image noise in chest CT. AJR 2014;203:123-130.

III Kaasalainen T, Palmu K, Lampinen A, Reijonen V, Leikola J, Kivisaari R, Kortesniemi M. Limiting CT radiation dose in children with craniosynostosis: phantom study using model-based iterative reconstruction. Pediatr Radiol, in press. doi: 10.1007/s00247-015-3348-2.

IV Nikupaavo U, Kaasalainen T, Reijonen V, Ahonen SM, Kortesniemi M. Lens dose in routine head CT: Comparison of different optimization methods with anthropomorphic phantoms. AJR 2015;204:117-123.

V Kelaranta A, Kaasalainen T, Seuri R, Toroi P, Kortesniemi M. Fetal radiation dose in computed tomography. Radiat Prot Dosimetry 2015;165:226-230.

The author participated in planning all the studies. Additionally, the author's contribution to these studies was: reviewing the literature, performing the dose and image quality measurements, analyzing the dose measurements, and writing the articles (Studies I-III), as well as carrying out simulations (Study III); constructing the study, performing the dose and image quality measurements, and co-writing the article (Study IV); and performing the dose measurements and co-writing the article (Study V). In addition, the author also drafted or revised and approved all the published manuscripts as required in the Vancouver Convention. The results of these studies do not appear in other Ph.D. theses.

ABBREVIATIONS

AAPM	American Association of Physicists in Medicine
ALARA	As low as reasonably achievable
ASIR	Adaptive Statistical Iterative Reconstruction (GE Healthcare)
CNR	Contrast-to-noise ratio
CT	Computed tomography
CTDI	Computed tomography dose index
$CTDI_{vol}$	Volume-weighted computed tomography dose index
D	Absorbed dose
DAP	Dose-area product
$d\bar{\varepsilon}$	Mean energy
DLP	Dose-length product
E	Effective dose
ESD	Entrance surface dose
FBP	Filtered back projection
FDA	U.S. Food and Drug Administration
FWHM	Full width at half maximum
H_T	Equivalent dose
HU	Hounsfield unit
IAEA	International Atomic Energy Agency
ICRP	International Commission on Radiological Protection
ICRU	International Commission on Radiation Units and Measurements
LAT	Lateral
MBIR	Model-based iterative reconstruction
MOSFET	Metal-oxide-semiconductor field-effect transistor
MSCT	Multislice CT
NCRP	National Council on Radiation and Measurements (USA)
OBTCM	Organ-based tube current modulation
OSLD	Optically stimulated luminescent dosimeter
PA	Posterior to anterior
PMMA	Polymethyl methacrylate
RANDO	Radiation Analogue Dosimetry system
ROI	Region of interest
RPLD	Radiophotoluminescent dosimeter
RQT	Standard radiation quality used to determine characteristics in CT applications
Safire	Sinogram Affirmed Iterative Reconstruction, a raw data-based iterative reconstruction of Siemens CT scanners
SD	Standard deviation
SFOV	Scan field of view
SSDE	Size-specific dose estimate

STUK	Radiation and Nuclear Safety Authority (Säteilyturvakeskus, Finland)
TCM	Tube current modulation
TLD	Thermoluminescent dosimeter
VEO	A model-based iterative reconstruction of GE Healthcare CT systems
w_R	Radiation-weighting factor for radiation type R
w_T	Tissue-weighting factor
X-CARE	An OBTCM technique of Siemens Healthcare CT systems

AIMS AND STRUCTURE OF THE THESIS

The purpose of this thesis was to study the feasibility of using anthropomorphic phantoms and metal-oxide-semiconductor field-effect transistors (MOSFETs) in computed tomography (CT) optimization, with special emphasis on pediatric patients, unborn children, and on radiosensitive organs. The first two papers of this thesis focused on proper patient centering on the CT scanner isocenter, which also serves as the basis for all further optimization practices in all CT examinations. In the third paper of this thesis, ultralow-dose CT protocols for craniosynostosis imaging were constructed and tested on two anthropomorphic head phantoms of different ages and sizes. The fourth article of this thesis concentrated on the optimization of head CT studies in order to reduce doses to the eye lens, while the last publication of this work assessed fetal radiation doses in the most common CT examinations of pregnant women which also place the fetus at the greatest risk for radiation-induced health detriments.

The specific goals of the research described in this thesis were:

1) to assess the effect of patient off-centering on patient dose and image quality in chest CT (Studies I, II)

2) to construct ultralow-dose CT protocols for craniosynostosis imaging, and to examine the feasibility of using model-based iterative image reconstruction to reduce organ and effective doses with this indication while maintaining sufficient image quality for diagnosis (Study III)

3) to study different CT optimization methods for reducing the organ doses to radiosensitive eye lenses in routine head CT examinations (Study IV)

4) to determine fetal doses in different stages of pregnancy in trauma, low-dose abdominopelvic and pulmonary angiography CT examinations, and to calculate relative doses between the $CTDI_{vol}$ and fetal doses (Study V)

- Study I

Kaasalainen T, Palmu K, Lampinen A, Kortesniemi M.
Effect of vertical positioning on organ dose, image noise and contrast in pediatric chest CT – phantom study
Pediatr Radiol 2013;43:673-684.

Chest CT scans of a five-year-old anthropomorphic phantom were performed in different patient vertical positions (offset from -6 cm to +5.4 cm with respect to the CT scanner isocenter) with a 64-slice CT scanner. Organ doses in seven different tissues were measured and estimated with MOSFET dosimeters. The CT number histograms corresponding to different tissues served to determine image noise and contrast. Mean absorbed organ doses for each off-centered patient vertical position were compared to the dose at the reference level and relative doses were calculated from the difference between the reference level and the off-centered vertical positions. Similarly, the image contrast and relative image noise in different tissues were determined in each patient vertical position and compared to the reference level.

- Study II

Kaasalainen T, Palmu K, Reijonen V, Kortesniemi M.
Effect of patient centering on patient dose and image noise in chest CT
AJR 2014;203:123-130.

Three different sized anthropomorphic phantoms from newborn to adult were scanned using different vertical patient centering (offset ± 6 cm with respect to the CT scanner isocenter) and either posterior-to-anterior or lateral scout images for automatic tube current modulation, following an evaluation with radiation dose-monitoring software. The effect of vertical positioning on radiation dose was studied with $CTDI_{vol}$, DLP and SSDE, and relative changes in the dose indices were compared to doses observed at the reference levels. Image noise was determined from CT number histograms, and the relative image noise of each vertical position was compared to a visually set reference level. In addition to phantom measurements, vertical offsets for 112 patients ranging from newborn to adult were retrospectively assessed.

- Study III

Kaasalainen T, Palmu K, Lampinen A, Reijonen V, Leikola J, Kivisaari R, Kortesniemi M.
Limiting CT radiation dose in children with craniosynostosis: phantom study using model-based iterative reconstruction
Pediatr Radiol, in press. doi: 10.1007/s00247-015-3348-2

Two anthropomorphic phantoms, corresponding to pediatric newborn and five-year-old patients, were scanned on a 64-slice CT scanner using different low-dose protocols for craniosynostosis. For this purpose, ultralow-dose CT

protocols that employ model-based iterative reconstruction were constructed. Organ doses in the head region were measured with MOSFET dosimeters, and doses of low-dose scans were compared to routine protocols for craniosynostosis. Additionally, simulations using the ICRP 103 tissue-weighting factors served to determine organ doses and effective doses. Three different iterative reconstructed image datasets (ASIR30%, ASIR50% and VEO) served to evaluate image quality. The CT number histograms of different tissues served to determine image noise and contrast, which were compared to routine CT protocols. Two experienced physicians evaluated subjective image quality in a blinded manner.

- Study IV

Nikupaavo U, **Kaasalainen T**, Reijonen V, Ahonen SM, Kortesniemi M.
Lens dose in routine head CT: Comparison of different optimization methods with anthropomorphic phantoms
AJR 2015;204:117-123.

Two anthropomorphic head phantoms were scanned with a routine head CT protocol of the brain using bismuth shielding, gantry tilting, organ-based tube current modulation (OBTCM), or their combinations. High-sensitivity MOSFET dosimeters served to measure local absorbed doses to the head region. ROI analysis served to determine the relative changes in image noise and contrast. The results of the dose and image quality measurements were compared to the routine head CT protocol without using any optimization technique.

- Study V

Kelaranta A, **Kaasalainen T**, Seuri R, Toroi P, Kortesniemi M. Fetal radiation dose in computed tomography
Radiat Prot Dosimetry 2015;165:226-230.

Different sized boluses representing the gestational ages of 12, 20, 28 and 38 weeks served to model four stages of pregnancy. The adult female anthropomorphic phantom, with MOSFET dosimeters placed inside the phantom, was examined with a 64-slice scanner in the three most common CT protocols used in emergency situations during pregnancy: trauma, abdominopelvic and pulmonary angiography. The average of the measured doses corresponding to uterus volume in each pregnancy stage served to determine the mean fetal dose. Additionally, relative doses were calculated between the mean fetal dose and mean $CTDI_{vol}$ for each pregnancy stage and protocol. A pulmonary embolism CT angiography scan was used to study the effect of scan range proximity on fetal dose.

1 INTRODUCTION

The development of multislice computed tomography (MSCT) scanners with helical imaging has greatly enhanced diagnostic capabilities and substantially reduced scanning times, making computed tomography (CT) scanning both patient-friendly and the physician's preferred tool in diagnosing many diseases. Consequently, the number of CT examinations performed worldwide has increased year after year, which has also raised the collective radiation dose accumulated from CT examinations [Hart and Wall 2004; Aroua et al. 2007; Børretzen 2007; Mettler et al 2008; Tenkanen-Rautakoski 2008; Bly et al. 2011; Dougeni et al 2012; Helasvuo 2013]. According to the recently published STUK report [Helasvuo 2013], approximately 3.6 million X-ray examinations, excluding dental X-ray examinations performed in dental surgery, took place in Finland in 2011. Of this number, approximately 9%, corresponding to 60 examinations per 1000 inhabitants, were CT scans of different body and head regions, and 1.7% were CT scans of pediatric patients. The most common CT studies included CT scans of the head, whole body, abdomen and thorax. In children, the most common CT studies involved CT scans of the head, thorax and cranial bones. Due to increased use, CT has become a major contributor to accumulated radiation doses from radiological examinations. Although fewer than one in ten X-ray studies currently performed in Finland is a CT study, they contribute to the nearly 60% of the collective effective radiation dose from medical examinations [Muikku et al. 2014], which is similar to or lower than that reported in other countries [Børretzen 2007; Paterson and Frush 2007; NRCP 2009; Dougeni et al. 2012; EC 2013]. In 2011, the estimated mean annual effective dose in Finland was 3.2 mSv, to which the estimated contribution of medical X-rays was 0.45 mSv [Muikku et al. 2014]. This figure is significantly lower than that in, for example, the US, which saw nearly 62 million CT examinations in 2006, corresponding to 207 CT examinations per 1000 population [NCRP 2009].

Although radiotherapy uses ionizing radiation for curative cancer treatments, radiation is also known to cause adverse health effects. These adverse effects of radiation on the human body fall into two categories: tissue reactions (previously deterministic effects) and stochastic effects. Tissue reactions (e.g. skin burns, cataracts, and erythema) originate from high absorption of radiation doses by tissues; below a certain threshold, such effects will be absent. The severity of the tissue reactions depends on the absorbed dose, and such reactions are exceedingly rare in CT, although some publications have recently reported a few cases [FDA 2010; Wintermark 2010]. Unlike for tissue reactions to radiation on the human body, no threshold has been established for ionizing radiation doses that cause stochastic adverse effects (including radiation-induced cancer or heritable effects), the severity of which is independent of the absorbed dose. However, the likelihood

of presenting with stochastic adverse effects is proportional to the dose absorbed by human tissues, and in accordance with current knowledge, the risk for stochastic effects from radiation (e.g. cancer) increases linearly with radiation dose [BEIR 2006; Brenner and Hall 2007; Berrington de González et al. 2009; Pearce et al 2012]. Furthermore, the lifetime attributable cancer risk among children from ionizing radiation is two to three times higher than the risk among adults, which the atomic bomb survival data estimate is 4-5% per sievert [Preston et al. 2007]. Additionally, the estimated stochastic cancer risk among women is higher than the risk among men with the same radiation dose levels, mainly due to the high sensitivity of breast tissue to ionizing radiation [Preston et al. 2007]. Because the stochastic effects of radiation have no established thresholds and may cause cancers or genetic mutations even at lower radiation doses, they have become a major focus of research on radiation protection and the optimization of radiological examinations. Specifically, the growing number of CT studies performed has driven interest in optimizing CT scan protocols [Kalra et al. 2004a; Kalender et al. 2008; Mettler et al. 2008; Nievelstein et al. 2010; Dougeni et al. 2012].

The objective of optimizing radiological examinations is to minimize the patient dose and stochastic harm to the population without compromising diagnosis, which means that the optimization task is to maximize the benefits of ionizing radiation while reducing the risk ratio for the diagnostic radiological examination. Optimization is always a two dimensional problem: the image quality should be adequate for diagnosis, but the patient dose should remain as low as reasonably achievable (ALARA) [ICRP 2007]. Achieving this goal will require multiprofessional work. One particular concern has focused on optimizing the CT scans of pediatric patients, as children are more sensitive to radiation exposure than are adults, and their life-expectancy is higher also; consequently, the expected radiation risk is higher for children under the same exposure settings as for adults [Brenner et al. 2001; Huda and Vance 2007; Preston et al. 2007; Deak et al. 2010; Nievelstein et al. 2010]. Several international campaigns have recently been launched in an effort to optimize CT practices, especially for children. The Alliance for Radiation Safety in Pediatric imaging, for example, launched their Image Gently campaign in the summer of 2007 (http://imagegently.dnnstaging.com/Home.aspx), and the European Society of Radiology launched its EuroSafe Imaging campaign in the spring of 2014 (http://www.eurosafeimaging.org). Finnish pediatric radiologists, together with the Radiation and Nuclear Safety Authority (STUK), published in 2012 on the STUK website the Finnish guidelines for pediatric CT, which include practical advices for optimizing pediatric CT examinations [STUK 2012]. Furtherfore, a recently published article from Finland introduced indication-based national reference levels as a function of patient weight for use in the most common pediatric CT examinations [Järvinen et al. 2015]. Similarly to optimizing pediatric CT examinations, efforts should also highlight the need to reduce the radiation exposure of radiosensitive organs, such as the thyroid gland, eye lenses and breast tissue.

Several technical and clinical approaches can promote effective CT optimization. Technical methods developed for this purpose include, for example, tube current modulation (TCM), lowered tube voltage, adaptive beam collimation, organ-based tube current modulation (OBTCM), the use of local exterior bismuth shielding and gantry tilt [Gies et al. 1999; Kalender et al. 1999; Hopper et al. 2001; Kalra et al. 2004b; McLaughlin and Mooney 2004; Heaney and Norvill 2006; Kalender et al. 2008; Deak et al. 2009; Tan et al. 2009; Suzuki et al. 2010; Duan et al. 2011; Wang et al. 2011; Yu et al. 2011; Reimann et al. 2012; Wang et al. 2012a; Hugget et al. 2013; Chatterson et al. 2014; Taylor et al. 2015]. Reducing the tube voltage, kVp, on iodine enhanced CT scans (e.g. for pulmonary embolism), significantly reduces the patient dose without compromising the diagnostic information of CT images thanks to the improved contrast of arteries [Sigal-Cinqualbre et al. 2004; Schueller-Weidekamm et al. 2006; Matsuoka et al. 2009; Yu et al. 2011]. Depending on the specific indication of the study, low-dose protocols may be preferable when higher noise levels do not compromise diagnostic quality [Udayasankar et al. 2009; Lee et al. 2011]. Recent innovations for CT optimization also include tools for image reconstruction with several types of iterative reconstruction algorithms [Thibault et al. 2007; Katsura et al. 2012; Pickhardt et al. 2012; Deák et al. 2013; Miéville et al. 2013; Smith et al. 2014; Greffier et al. 2015; Hérin et al. 2015; Padole et al. 2015a; Padole et al. 2015b; Samei and Richard 2015; Widmann et al. 2015]. The availability of several new effective technical tools for CT optimization does not reduce the importance of preparing and positioning the patient on the CT scanner isocenter, and other user-related optimization practices.

Because assessing radiation dose has become an important task for managing CT exposures and optimizing CT studies, the need to develop more accurate methods for this purpose has become more acute. Previously, patient dose estimates were typically based on dose measurements taken with cylinder-shaped body and head phantoms and ionization chambers. However, the failure of this standardized $CTDI_{vol}$ method to take into account patient size and attenuation properties has driven the development of other methods. CT doses at various body locations are assessable experimentally with phantom measurements or computationally through Monte Carlo simulations [Brix et al. 2004; Bostani et al. 2014; Tian et al. 2014; Tian et al. 2015]. Experimental dose measurements are usually carried out with anthropomorphic phantoms designed to permit the placement of small dosimeters at various locations corresponding to different organs and tissues. These tissue-equivalent anthropomorphic phantoms composed of materials that simulate typical soft and bone tissues, such as cartilage, the spinal cord and disks, lung, brain and sinuses, and can simulate real patients. They are also beneficial in user training and CT protocol optimization after installing new CT equipment. On the other hand, computer programs can also simulate radiation transport inside mathematical or voxel-based phantoms.

2 PATIENT DOSIMETRY AND CT OPTIMIZATION

2.1 CT OPTIMIZATION

2.1.1 TUBE CURRENT MODULATION AND BEAM-SHAPING FILTERS

In radiological examinations, the number of X-ray photons detected is directly proportional to the tube current-time product (in CT, the tube current-rotation time product) value, mAs. In CT, the image noise is inversely proportional to the square root of the radiation dose, and thus mAs, which comes from the Poisson distribution of detected X-ray photons. Thus, the most straightforward dose reduction and optimization method in CT imaging is to reduce the mAs used in scanning.

Previously, CT scanning used fixed tube currents, but because patient size and the attenuation properties of different tissues impact the overall X-ray attenuation, and thus also dose distribution, CT manufacturers nowadays equip their MSCT scanners with 3D TCM features. The aim of TCM is basically to maintain the image quality (noise level) standard in the scanned volume regardless of patient size [Gies et al. 1999; Kalender et al. 1999; Kalra et al. 2004b; Kalender et al. 2008]. Thus, TCM techniques serve to increase the tube current for more attenuating areas and to decrease the tube current for less attenuating areas. Although the goals are the same, the principles of TCM methods differ across CT scanners from different manufacturers [Sookpeng et al. 2014], so knowledge of the relationships between patient size, dose and image noise is important for CT optimization. As a general rule of thumb and depending on the tissue composition and its attenuation properties in the energy of a particular X-ray beam, if a patient's diameter increases by 4-8 cm, but same image quality is needed, the operator must double the mAs [Hubbel and Seltzer 2004].

In addition to TCM techniques, CT scanners include bowtie filters to spatially shape the X-ray field intensity within the scan field of view (SFOV), and thus to compensate for patient attenuation at the detector-signal level [Toth et al. 2007]. The function of a bowtie filter is to allow maximum X-ray intensity on the thickest part of a patient, which also attenuates the most X-rays, while reducing X-ray intensity in peripheral areas with less attenuation, thereby reducing X-ray scatter and the radiation dose to surface tissues [Toth 2002]. The optimal function of the bowtie filter and TCM techniques assumes the patient's axial center of mass is centered at the scan isocenter [Li et al. 2007; Toth et al. 2007; Gudjonsdottir et al. 2009; Matsubara et al. 2009; Habibzadeh et al. 2012]. The impact of patient positioning errors on radiation dose and image quality is the subject of publications I-II in this thesis.

Recent technical innovations in CT also include organ-based tube current modulation (OBTCM), which can reduce doses in superficial radiosensitive tissues [Duan et al. 2011; Reimann et al. 2012; Wang et al. 2012a; Taylor et al. 2015]. OBTCM methods aim to reduce radiation exposure anteriorly at certain limited angles of tube rotation. Angles and dose reduction percentages differ depending on the CT vendor. Similarly, some systems boost radiation output on the patient's posterior side to obtain sufficient level of image noise, whereas others offer no compensation for anteriorly produced dose reduction at all. Study IV of this thesis explored the feasibility and benefits of using OBTCM to reduce the radiation dose to the eye lenses.

2.1.2 TUBE VOLTAGE

Radiation dose depends not only on mAs level, but also on the peak tube voltage. Increasing the kVp also increases the radiation dose because the radiation beam then carries more energy. Of course, reducing the kVp will decrease the output of the X-ray tube and thus reduce the radiation dose to the patient. However, inappropriately reducing the tube voltage may markedly increase X-ray attenuation in tissues and increase image noise, particularly in large patients. Consequently, larger and more obese patients may have experienced higher tube voltages, since a higher kVp increases the intensity of the X-rays penetrating the patient in order to reach the detectors. The radiation output of the X-ray tube relates to the tube voltage in CT by a factor of approximately $U^{2.5}$, where U is the peak tube voltage [Brix et al. 2004; IAEA 2014].

Recently, kVp optimization has become one of the most active areas in the field of CT optimization. The greatest benefits of lowering the kVp are achieved in contrast-enhanced CT examinations and in the CT scans of small and pediatric patients [Yu et al. 2011]. Lowering the kVp decreases photon energy, causing greater absorption by iodinated contrast media and thus increasing the contrast between the artery lumen and surrounding tissues. Additionally, because patient size significantly affects X-ray attenuation and because children are smaller in size, the CT acquisition parameters for children should not be the same as for adults. Due to their smaller size, and thus their lower attenuation of radiation, pediatric patients can typically be scanned at lower kVp values than those used for adults. Because optimizing the kVp in clinical routine can be difficult, CT manufacturers have begun to develop automatic tube voltage selection tools for adjusting the kVp to suit the individual patient's attenuation properties and clinical tasks. The main goal of these methods is to maintain a consistent contrast-to-noise ratio (CNR) while scanning at a minimal dose level for the patient. These tools have helped substantially to reduce patient doses without compromising image quality in various patient sizes [Schindera et al. 2013].

2.1.3 ITERATIVE IMAGE RECONSTRUCTION

Recent, partially newly found innovations for CT optimization also include tools for image reconstruction with several types of iterative reconstruction algorithms [Thibault et al. 2007; Katsura et al. 2012; Pickhardt et al. 2012; Deák et al. 2013; Miéville et al. 2013; Smith et al. 2014; Greffier et al. 2015; Hérin et al. 2015; Padole et al. 2015a; Padole et al. 2015b; Samei and Richard 2015; Widmann et al. 2015]. Iterative image reconstruction, though already common in the early years of CT, was discouraged when the amount of measured data increased, causing higher computational demands with iterative reconstruction than with more analytical methods [Beister et al. 2012]. Nevertheless, the higher computational capacities of recent workstations, algorithm developments, and ongoing efforts to lower radiation exposure in CT have made it a hot CT optimization topic again in the past ten years.

Iterative image reconstruction algorithms use multiple repetitions in which the current solution converges towards a better solution [Beister et al. 2012]. Depending on the iterative reconstruction technique, a notable dose reduction (of up to 90%) over that of filtered back projection (FBP) reconstruction may be possible by taking advantage of the physical characteristics of the imaging system, and thus modelling the acquisition process more precisely as well as improving image quality by reducing image noise [Katsura et al. 2012; Pickhardt et al. 2012; Deák et al. 2013; Miéville et al. 2013; Smith et al. 2014 ; Greffier et al. 2015; Hérin et al. 2015; Padole et al. 2015a; Samei and Richard 2015]. Different CT manufacturers use several iterative reconstruction techniques [Padole et al. 2015a]. Statistical reconstruction methods, for example, model the counting statistics of the photons detected by respective weighting of the X-rays measured, whereas the model-based iterative reconstruction (MBIR) technique uses a complex system of prediction models, including the modeling of optical factors such as X-ray tubes and detector responses as well as voxel projections, X-ray beam spectra and noise modeling, to improve the simulation of the acquisition process [Thibault et al. 2007; Beister et al. 2012].

MBIR has proved to be the most efficient dose reduction technique of all iterative reconstruction techniques and is especially suitable for lower radiation doses, as it reduces image noise more effectively than other reconstruction methods do. Thus, MBIR may escape from the statistical effect, which states that noise is inversely proportional to the square root of the radiation dose, by employing a more correct and intricate physical model in its iteration process. Several studies, concerning mainly chest and abdominal CT, have shown that MBIR can reduce patient doses more effectively than can FBP or first-generation iterative reconstruction methods while preserving or improving image quality [Katsura et al. 2012; Pickhardt et al. 2012; Deák et al. 2013; Miéville et al. 2013; Smith et al. 2014; Hérin et al. 2015; Padole et al. 2015a; Samei and Richard 2015]. However, Padole et al. (2015b) warned that it is possible to miss clinically significant lesions (< 8 mm) in abdominal CT examinations acquired at ultralow-dose levels. Similarly, Samei and Richard

(2015) noted that MBIR may show reduced performance for low-contrast tasks at low doses, which may influence low-contrast object detectability, such as focal infectious diseases, in very low-dose conditions. Additionally, iterative reconstruction techniques (especially MBIR) alter the image texture, and the noise power spectrum (NPS) tends to shift to lower frequencies [Samei and Richard 2015]. A very recent paper has also demonstrated the dose-reduction capabilities of MBIR in CT examinations of craniofacial bones [Widmann et al. 2015]. Study III of this thesis explored the use of MBIR.

2.2 PATIENT DOSIMETRY IN CT

Patient dosimetry is considered an integral part of a quality assurance program in radiology [STUK 2006; IAEA 2007; STUK 2008]. Patient dosimetry aims to quantify the radiation exposure absorbed by the body. The absorbed dose, *D*, represents the mean energy, $d\bar{\varepsilon}$, imparted to matter per unit mass, *m*, by ionizing radiation (Equation 1) [Attix 1986].

$$D = \frac{d\bar{\varepsilon}}{dm} \tag{1}$$

The special name for the unit of the absorbed dose is the gray (Gy).

Due to the substantially different dose distribution of CT from that of conventional projection radiography, special dose quantities are needed. In projection radiography, entrance surface dose (ESD) and dose-area product (DAP) serve as physical dose estimates when quantifying the magnitude of the patient's exposure to ionizing radiation, whereas CT uses the computed tomography dose index (CTDI), or more commonly, the volume-weighted CTDI ($CTDI_{vol}$), and dose-length product (DLP). The $CTDI_{vol}$ represents the mean weighted dose absorbed by the imaged volume, whereas the DLP represents the total energy absorbed into the body (and thus more accurately estimates the stochastic risks of radiation on the human body) when acquiring a complete stack of CT images. Calculation of these dose indices is based on measurements with ionization chambers and standardized cylindrical homogeneous PMMA (polymethyl methacrylate) phantoms – either a 16-cm head phantom or a 32-cm body phantom – simulating the patient's attenuation. However, because patient sizes and compositions vary among patients and scanned body regions, the use of CTDI and DLP may be subject to significant uncertainties. The $CTDI_{vol}$ provides information only about the scanner radiation output and does not address patient size; consequently, it does not estimate the actual patient dose [McCollough et al. 2011]. The American Association of Physicists in Medicine (AAPM) recently published a corrective method for this problem with patient size, suggesting that the use of size-specific dose estimates (SSDE) more accurately estimates the patient dose [AAPM 2011]. This practice is important, especially for pediatric CT or when scanning small adults, as using a 32-cm cylindrical phantom as a reference in $CTDI_{vol}$ calculations may lead to the underestimation of patient dose levels by

a factor of two to three [AAPM 2011]. However, the SSDE calculation method of AAPM based on effective diameter is not optimal, as it does not take into account patient attenuation properties; as a result, some have suggested replacing it with an attenuation-based size metric known as the water equivalent diameter [Wang et al. 2012b; Wang et al. 2012c; Bostani et al. 2015a]. Furthemore, although CTDI and SSDE can guide the improvement of clinical practice, they should not be used to assess individual patients' risk from CT examinations [AAPM 2011].

In addition to $CTDI_{vol}$, SSDE, and DLP patient dosimetry practices, absorbed doses at various locations can be assessed more accurately experimentally using direct dose measurements or computationally through Monte Carlo simulations [Brix et al. 2004; Deak et al. 2010; Bostani et al. 2014; Tian et al. 2014; Tian et al. 2015].

2.2.1 EQUIVALENT DOSE (H_T) AND EFFECTIVE DOSE (E)

The probability of stochastic radiation effects has been found to depend not only on the absorbed dose, but also on the type and energy of the radiation and the tissue or organ exposed to the radiation [ICRP 1991; ICRP 2007]. The equivalent dose (H_T) and effective dose (E) serve as protective quantities for ionizing radiation. The equivalent dose serves to assess the extent of biological damage expected from the absorbed dose and takes into account the radiation type and energy (Equation 2).

$$H_T = \sum_R w_R D_{T,R}, \tag{2}$$

where w_R is the radiation-weighting factor for radiation type R, and $D_{T,R}$ is the absorbed dose by tissue T. For X-rays used in clinical radiology, $w_R = 1$, so the absorbed organ dose (Gy) equals the equivalent dose (a sievert, Sv). The effective dose represents the stochastic health risk, or the probability of cancer induction and genetic effects that ionizing radiation delivers to irradiated body parts. The effective dose is the tissue-weighted sum of equivalent doses in all specified tissues and organs of the body (Equation 3).

$$E = \sum_T w_T H_T, \tag{3}$$

where w_T is the tissue-weighting factor for tissue or organ T, the sum of which is equal to 1, and H_T is the equivalent dose for tissue or organ T. Similarly to the equivalent dose, the effective dose is also given in sieverts. The International Commission on Radiological Protection (ICRP) regularly updates tissue-weighting factors in light of new knowledge about the sensitivities of different tissues to ionizing radiation. The most recent revisions (Table 1) date from 2007 with the publication of the ICRP 103 report that gives the updated factors from the ICRP 60 report [ICRP 1991; ICRP 2007]. E is based on the detriment to a population of all ages and averaged across the both genders. Thus, E does not relate directly to an individual patient's relative cancer risk, as patients are known to differ in age and gender. For individual risk

assessments, the equivalent dose should serve as a reference protective quantity, and *E* should serve only to compare different health detriments to a reference patient for various types of diagnostic examinations [ICRP 2007].

The effective dose can be roughly estimated in CT with Monte Carlo-based conversion factors from DLP to *E* or be determined with computer simulations or measurements with phantoms.

Table 1 – Tissue-weighting factors, w_T, according to the ICRP 60 and ICRP 103 reports on determining the effective dose.

Organ/tissue	Tissue-weighting factor	
	ICRP 60	ICRP 103
Bone marrow, colon, lung, stomach	0.12	0.12
Breast	0.05	0.12
Gonads	0.20	0.08
Bladder, liver, esophagus, thyroid	0.05	0.04
Bone surfaces, skin	0.01	0.01
Brain, salivary glands	-	0.01
Remainder*	0.05	0.12
Total	**1.00**	**1.00**

* The ICRP 103 [ICRP 2007] and ICRP 60 [ICRP 1991] reports list the remainder tissues and different calculation methods for assessing $D_{remainder}$. According to the ICRP 103 report, remaining tissues currently include: the adrenals, extrathoracic tissue, gall bladder, heart wall, kidneys, lymph nodes, muscle, oral mucosa, pancreas, prostate, small intestine, spleen, thymus, and uterus/cervix.

2.2.2 DOSIMETER TYPES

Dosimeters serve to detect and measure an individual's or an object's exposure to radiated energy from ionizing radiation. Several different types of dosimeters are used to measure the amount of radiation; some serve in personnel dosimetry and others in patient dosimetry, quality assurance or the optimization of examinations. However, the basic idea behind dosimeters is the same: measuring the energy released by the radiation requires an interaction between the radiation and the material.

Ionization chambers often serve quality assurance purposes in radiology. They consist of electrodes with a gas cavity in between. The radiation ionizes the gas particles, and the charged particles then move in the electrical field, and the electrodes collect them. By measuring this accumulated charge, one can determine the radiation dose. In CT, the ionization chambers serve mainly for CTDI measurements with cylindrical standardized phantoms, which partly limits their use for optimization purposes. In CT optimization (as well as in other examinations that use radiation) and organ and effective dose measurements, thermoluminescent dosimeters (TLD), optically stimulated luminescent dosimeters (OSLD), metal-oxide-semiconductor field-effect transistors (MOSFETs) and radiophotoluminescent dosimeters (RPLD) can serve to determine the amount of absorbed dose [Yoshizumi et al. 2007;

Zhang et al. 2013; Manninen 2014a]. A brief description of the general properties and working principles of TLD and MOSFET dosimeters appears below. More advanced theory on these, RPLD, OSLD and other dosimeters used in dosimetry are available in the literature [e.g. Attix 1986; Aschan 1999; IAEA 2005; IAEA 2007; Manninen 2014a].

TLDs measure ionizing radiation exposure by measuring the intensity of visible light that is emitted from a crystal in the detector when the crystal is heated [e.g. Cameron et al. 1968; Aschan 1999]. As the radiation interacts with the crystal material (usually lithium fluoride), it causes electrons in the crystal's atoms to jump to higher metastable energy states, where they are trapped due to intentionally introduced impurities in the crystal. Heating the crystal causes the electrons to drop back to their ground state, thereby releasing a photon of energy equal to the energy difference between the higher energy state and the ground state. The intensity of the emitted light is related to the amount of radiation exposure, which makes TLDs suitable for dosimetry. Moreover, the intensity of the emitted light is a function of the reading temperature; TLD chips are therefore read by measuring this intensity as a function of temperature. The radiation dose will typically be calibrated to the area of glow curves given by this process [Attix 1986]. The use of TLDs is time-consuming as dosimeters must be removed from an irradiated object before reading the values. The OSLDs and RPLDs basically function similarly to TLDs, except instead of heat, light of a specific wavelength (from a laser) releases the trapped energy in the form of luminescence [IAEA 2005].

For an instantaneous readout after irradiation, and thus more efficient working practices, MOSFET dosimeters can measure the radiation exposure [Soubra et al. 1994; Yoshizumi et al. 2007]. MOSFET dosimeters consist of a silicon semiconductor substrate, an insulating layer of silicon dioxide, and a metal gate (Figure 1). Its function rests on the principle that ionizing radiation produces changes in the charge carrier trapping such that a change in the threshold voltage required to induce a source-to-drain current flow occurs after irradiation rather than prior to irradiation [Knoll 2000]. Exposure to ionizing radiation causes electron-hole pairs to form in the silicon dioxide layer immediately below the gate. Applying a positive bias voltage to the gate during exposure tends to separate these charges, and electrons move toward the gate, and the holes toward the silicon dioxide-silicon interface where they will be trapped and form a fixed positive charge. This will induce a shift to more negative values in the threshold gate voltage. As an important task, the assessed change in threshold voltage is proportional to the absorbed dose. Moreover, the higher the bias voltage, the greater the fraction of the charges collected will be, thus resulting in higher sensitivity. The other benefits of MOSFET dosimeters, in addition to real-time readout capability, include their small physical size, permanent post-radiation signal storage and dose rate independence, particularly low-energy dependence, good reproducibility and high sensitivity, and good linearity [e.g. Yoshizumi et al. 2007; Koivisto et al. 2013a; Koivisto et al. 2015]. However, MOSFET dosimeters tend to show

significant angular dependency, which is considerably smaller in soft tissues than free-in-air due to the smoothing effect of radiation scatter in tissues [e.g. Koivisto et al. 2013b].

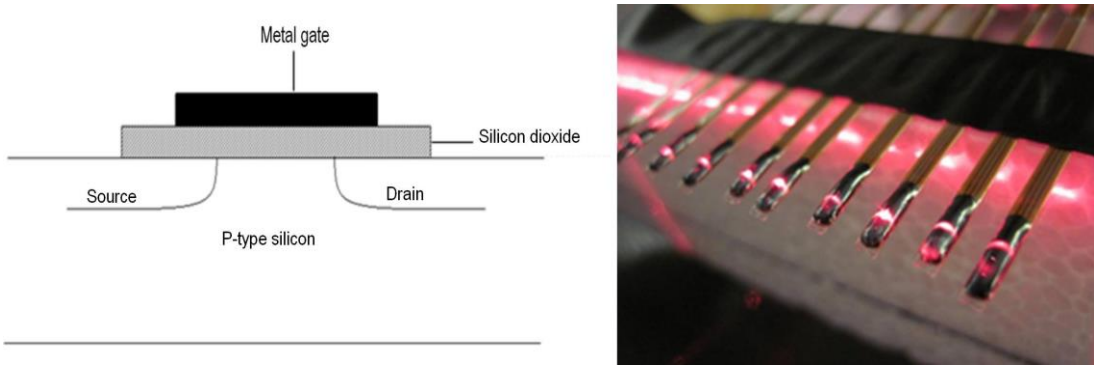

Figure 1 Configuration of a MOSFET dosimeter (left) and calibration setup for MOSFET dosimeters (right) showing the small size of the active parts and epoxy bulb of the MOSFET dosimeters.

2.2.3 ANTHROPOMORPHIC PHANTOMS

Because performing organ dose (or effective dose) measurements *in vivo* is impossible in practice, evaluating the stochastic health risks of ionizing radiation requires other methods. Patient dosimetry uses several different kinds of phantoms, the simplest of which are cylindrical and made from homogeneous PMMA material. However, these phantoms correspond only roughly to the human body or head and are unsuitable for organ dosimetry. Consequently, researchers have developed more advanced phantoms that more accurately simulate the way in which the patient absorbs and scatters ionizing radiation. Experimental dose measurements are usually carried out with different-sized anthropomorphic phantoms of both sexes that simulate real patients of different ages, and are designed to permit the placement of small dosimeters at various locations corresponding to different organs. These tissue-equivalent anthropomorphic phantoms composed of materials that simulate, for example, typical soft and bone tissues, such as cartilage, the spinal cord and disks, lung, brain and sinuses. Additionally, some of the anthropomorphic phantoms may consist of a real human skeleton. In this thesis, most of the studies were performed only with ATOM phantoms of different sizes (CIRS, Norfolk, USA): a pediatric newborn phantom (ATOM Model 703-D), a pediatric five-year-old phantom (ATOM Model 705-D), and an adult female phantom (ATOM Model 702-D), although Study IV also used a RANDO head phantom with a real human skull (The Phantom Laboratory, Salem, NY, USA) in the dose assessments. These phantoms were selected because they simulate the attenuation properties of real patients, contain dosimetry holes for several different organs, and are frequently used in the field of medical exposures.

2.2.4 MONTE CARLO SIMULATIONS

Monte Carlo simulations have seen wide use in radiation physics to solve medical dosimetric problems [Rogers 2006]. Such computer simulations have served in the planning of external beam radiotherapy and brachytherapy, in nuclear medicine, in diagnostic X-ray applications and in the calculation of radiation protection quantities. In patient dosimetry, the Monte Carlo method helps to determine the energy deposition of X-ray photons by simulating random interactions between radiation particles and the medium in order to create a trajectory of virtual radiation particles. A comprehensive review of Monte Carlo simulations in patient dosimetry appears in ICRU (2005). Simulations make it possible to determine the organ doses in different tissues and to calculate effective dose. To be precise, however, the voxel-based Monte Carlo simulation requires detailed modeling of the CT scanner and patient anatomy [Gu et al. 2009; Ding et al. 2012; Lee et al. 2012; Tian et al. 2014; Bostani et al. 2014; Bostani et al. 2015a; Bostani et al. 2015b; Tian et al. 2015]. Although modeling the CT scanner is difficult, it is doable. However, because modeling the patient's anatomy is even more difficult, most studies have used only a small number of computational phantoms. Because patient sizes and tissue or organ locations vary, modeling patient anatomy does not reflect the possible influence of anatomic variability across patients. However, the number of Monte Carlo models is increasing, and the XCAT phantom family, for example, now includes many different morphological patient models ranging from newborn to different-sized adults [Segars et al. 2010; Segars et al. 2013; Norris et al. 2014; Tian et al. 2015]. Furthermore, with XCAT phantoms, Tian et al. (2015) developed a quantitative model to prospectively predict organ doses for clinical chest and abdominopelvic scans which agreed closely with the retrospectively simulated organ doses for all organs. Study III of this thesis used the CT-Expo v.2.01 Monte Carlo simulation program (Georg Stamm and Hans Dieter Nagel, Hannover, Buchholz, Germany, 2001-2011) to determine organ doses and effective doses. This program is an MS Excel application written in Visual Basic that calculates doses resulting from CT examinations and is based on computational methods used in the 1999 German CT survey [Nagel et al. 2002]. It also includes dose calculations performed with different CT scanners for all age groups ranging from infants to adults, as well as a separate calculation for each gender. Brix et al. (2004) describes a theoretical formalism for the dose calculation, CT scanner, X-ray beam and phantom modeling used in CT-Expo, as well as uncertainties in the dose calculations.

3 MATERIALS AND METHODS

3.1 PATIENT CENTERING

In Studies I-II, we examined the effect of patient centering on patient dose and image quality. In Study I, a pediatric five-year-old anthropomorphic phantom was scanned at different table height positions using a chest CT protocol and the organ doses to different tissues in the chest area were determined using fourteen MOSFET dosimeters (standard TN-502RD and high sensitivity TN-1002RD MOSFET dosimeters with high bias settings, both from Best Medical, Canada) with active volumes of $2*10^{-5}$ mm^3. A fixed and up-scaled tube current served to reach sufficient reproducibility with MOSFET dosimeters. Prior to Study I, MOSFETs were calibrated in the STUK laboratory for 100 kVp with radiation quality reference RQT8 [IEC 2005]. For Studies III-V, MOSFETs were calibrated in a clinical CT beam in axial scanning mode for the energies used in the dose measurements. In calibrations, we measured the reference air kerma values with a RaySafe Xi CT pencil ionization chamber (Unfors RaySafe AB, Billdal, Sweden) and defined the calibration factor separately for each MOSFET dosimeter. The standard deviations of the repeated measurements in calibrations typically fell in the range of 2-5%. In Study II, we scanned three anthropomorphic phantoms of different sizes without MOSFET dosimeters with clinically used chest CT protocols. The effect of patient centering on patient dose was examined following an evaluation with radiation dose-monitoring software (DoseWatch, version 1.2, GE Healthcare, Milwaukee, Wisconsin, USA). In Studies I-II, the image quality was evaluated from the Hounsfield unit (HU) histograms of CT images without MOSFET dosimeters using an in-house-built Matlab (The MathWorks Inc., Natick, MA, USA) program (Figure 2). The contrasts between different tissues were determined from the locations of HU histogram peaks compared to those of water (0 HU) and image noise was calculated from the full width at half maximum (FWHM) values of the HU histogram peaks. In Study I, also the noise difference maps between centered and off-centered positions were created.

In addition to phantom measurements, the magnitude of patient miscentering (geometrically determined from the scout images) in five different clinical patient groups (112 patients altogether) was explored with dose-monitoring software, and their SSDE values were determined.

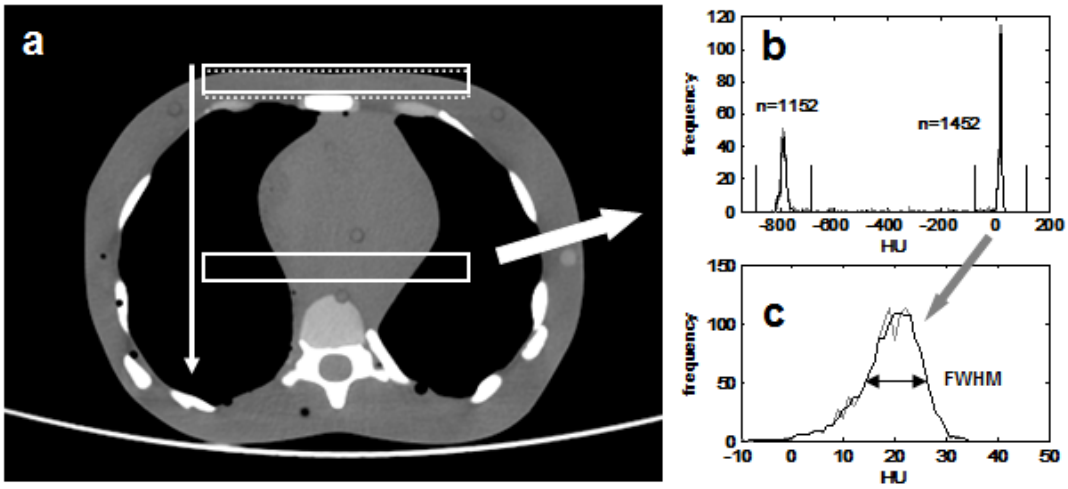

Figure 2 The methodology used to determine image quality. **a)** Schematic presentation of the calculation of the noise matrix where a region of interest (ROI) is shifted through each image along the y axis. **b)** In each ROI, a median-filtered histogram (black line) is divided into windows, and the contributions of each material are calculated (this particular image contains no bone). **c)** FWHM is evaluated from the peak of the most common material in the ROI (Studies I-III).

3.2 OPTIMIZING CRANIAL CT STUDIES

3.2.1 USE OF MODEL-BASED ITERATIVE RECONSTRUCTION FOR CRANIOSYNOSTOSIS CT

Studies III-IV examined the optimization of head CT examinations. In Study III, we constructed low-dose and ultralow-dose craniosynostosis CT protocols utilizing lowered tube voltages, increased noise indices for TCM and also different iterative image reconstructions (ASIR30% (Adaptive Statistical Iterative Reconstruction), ASIR50% and VEO model-based iterative reconstruction) and scanned pediatric newborn and five-year-old anthropomorphic head phantoms on a 64-slice CT scanner (GE Discovery CT750 HD, GE Healthcare, Milwaukee, WI, USA). We used high-sensitivity MOSFET dosimeters (TN-1002RD) with high bias settings to determine organ doses for different tissues in the head region, or in the vicinity of it. Additionally, we compared the doses of low-dose protocols to those of routine CT protocols for craniosynostosis. Furthermore, we performed Monte Carlo simulations with the CT-Expo computer program using similar low-dose parameters to those in MOSFET measurements. The organ doses to radiosensitive tissues and effective doses were determined and compared to routine protocols.

Objective image quality was determined using HU histogram analysis, as in Studies I-II, and the image contrast and noise were estimated from the locations and FWHMs of the HU histogram peaks. Results were then compared to scan protocols used in clinical routines for craniosynostosis. Two experienced, board-certified pediatric physicians used a five-point Likert scale [Likert 1932] to evaluate the subjective image quality in a blinded manner.

3.2.2 REDUCING EYE LENS DOSES IN ROUTINE HEAD CT EXAMINATIONS

Eye lenses are one of the most radiosensitive tissues and merit protection from ionizing radiation. In Study IV, we scanned two tissue-equivalent anthropomorphic head phantoms – ATOM (Model 703-D, CIRS, Norfolk, USA) and RANDO (The Phantom Laboratory, Salem, NY, USA), shown in Figure 3 – on a 128-slice CT scanner (Siemens SOMATOM Definition AS+, Siemens Healthcare, Erlangen, Germany) in helical mode with eight different scan optimization settings to reduce radiation exposure to the eye lenses: a reference scan with no optimization methods, with gantry tilted according to clinical practice (baseline from the skull base to the radix nasi), gantry tilted at half the angle used in clinical practice, with a 0.06-mm Pb bismuth shield (AttenuRad Radiation Protection, F&L Medical Products, Vandergrift, PA, USA) over the eyes, with both a bismuth shield and gantry tilted according to clinical practice, with OBTCM (X-CARE, Siemens Healtcare), with both OBTCM and gantry tilted according to clinical practice, and with a bismuth shield set over the eyes already during scout imaging. Organ doses to the head region were measured with high-sensitivity MOSFET dosimeters (TN-1002RD) with high bias settings.

Figure 3 Anthropomorphic head phantoms used to assess radiation exposure to the eye lenses in a routine head CT. **a)** ATOM Model 703-D, **b)** RANDO (Study IV).

A manual ROI (region of interest) analysis was used to measure the image quality with an ATOM phantom with no MOSFET dosimeters placed inside the phantom. Image contrast and noise were determined by measuring the mean CT number value and the standard deviation (1 SD) of the CT number, respectively. The ROIs were drawn in selected locations of particular clinical significance (right cerebellum, anterior temporal lobes and basal ganglia

nuclei). Lastly, both the image quality and organ doses to different tissues were compared to those used in routine head CT protocol with no optimization method.

3.3 FETAL DOSES IN DIFFERENT STAGES OF PREGNANCY IN THE MOST COMMON EMERGENCY CT EXAMINATIONS DURING PREGNANCY

In Study V, we scanned an anthropomorphic adult female phantom (CIRS ATOM 702-D, Norfolk, USA), with gelatin boluses (Figure 4) constructed to simulate different stages of pregnancy (20, 28 and 38 weeks), in helical mode using trauma, low-dose abdominopelvic and pulmonary angiography CT protocols. A phantom with no bolus represented the pregnancy stage of 12 weeks and non-pregnant women. Ten MOSFET dosimeters served to measure the absorbed doses (a description of the MOSFET places appears in Figure 1 of Study V). We determined the mean fetal dose by averaging the measured doses corresponding to the uterus volume in each stage of pregnancy. Additionally, we calculated the relative doses between the $CTDI_{vol}$ and mean fetal dose for each stage of pregnancy and protocol, and presented them as a function of gestational age. Furthermore, we studied the effect of scan range proximity on fetal dose in pulmonary embolism CT angiography scans.

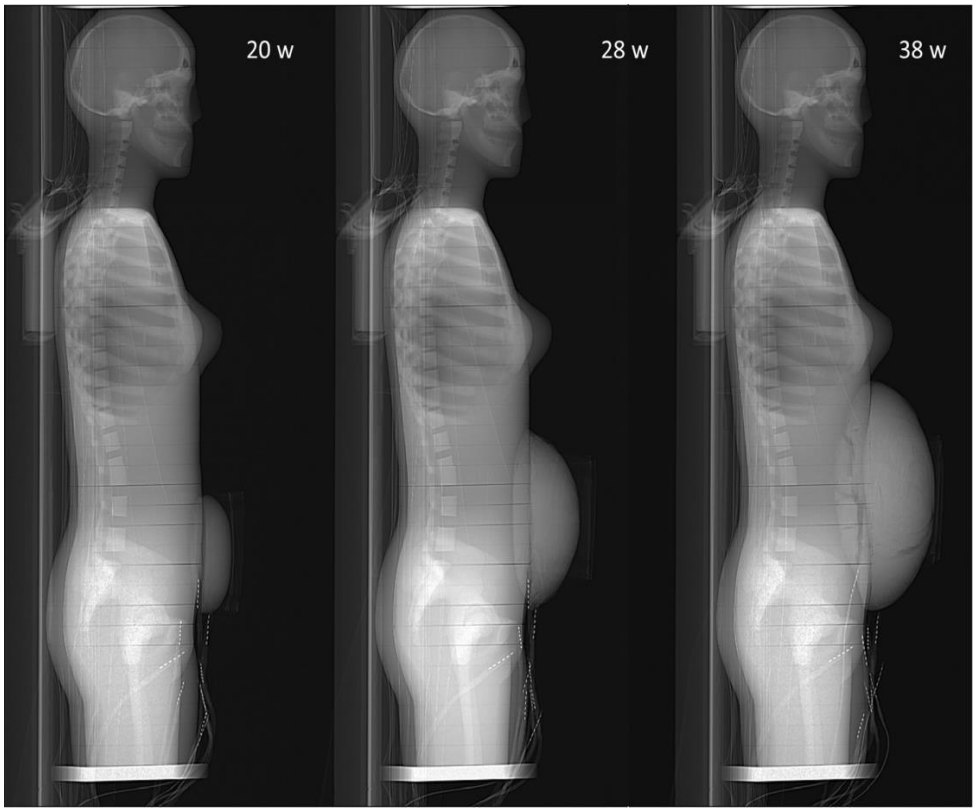

Figure 4 Lateral phantom scout projection images showing gelatin boluses modeling weeks 20, 28 and 38 of pregnancy (Study V).

4 RESULTS

4.1 PATIENT CENTERING

The results of Studies I-II showed that patient vertical off-centering is a common and serious problem in chest CT regardless of patient size. The evaluation of clinical patient examinations in Study II reveals that a majority of the patients scanned were positioned too low with respect to the isocenter of the CT scanner (Figure 5). The analysis with dose-monitoring software showed that the typical vertical offset for small patients was greater than for larger patients, with median values ranging from 25 to 35 mm below the isocenter. However, lateral centering showed no variation between patient groups, and median shifts from the isocenter were rare.

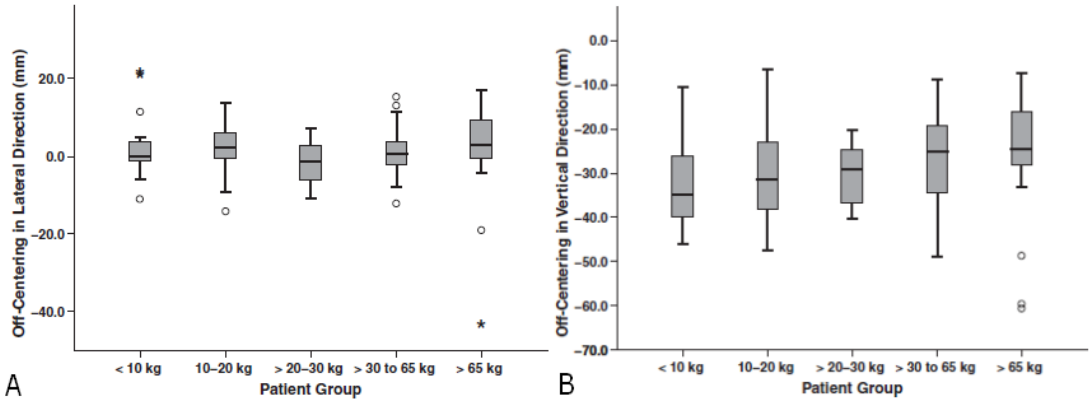

Figure 5 Lateral **a)** and vertical **b)** off-centering of the patients from the scan isocenter in different patient groups. The bottom and top of the boxes in the boxplots represent the first and third quartiles, and the band inside the boxes represents the median. The whiskers correspond to the most extreme point that remains within the first quartile - 1.5*(IQR) and third quartile + 1.5*(IQR) ranges. The small circles and stars represent mild and extreme outliers that fall either above or below the extreme points. Smaller and thinner patients were typically positioned lower than larger patients (p = 0.040) (Study II).

Based on Study I, doses to organs in phantoms varied significantly due to differences in vertical positioning, especially to radiosensitive anterior organs (Figure 6). The breast dose increased as much as 16%, and the thyroid dose as much as 24% in lower table height positions. Similarly, with the fixed mAs levels used in Study I, image noise increased 45% relative to the center position in the highest and lowest vertical positions with a particular increase on the anterior and posterior sides, respectively. Off-centering also affected the image contrast measured (up to 10 HU in soft tissue), which is important to know when measuring quantitative HU for differential diagnostics.

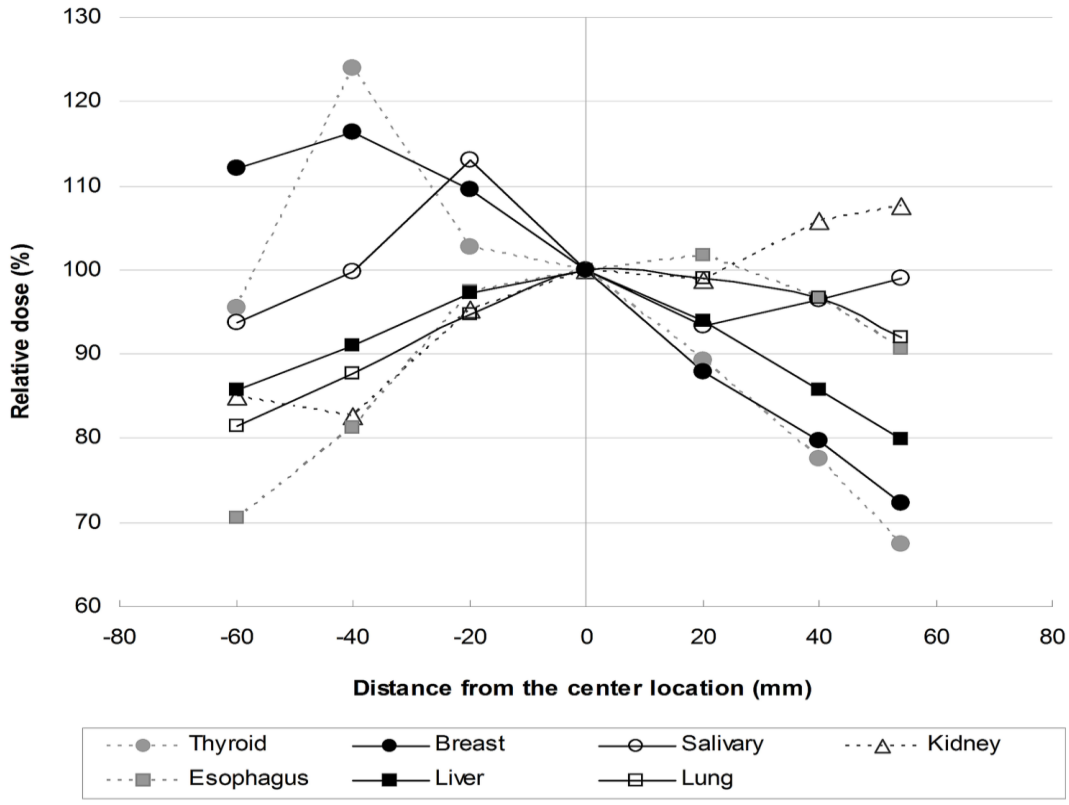

Figure 6 Mean relative organ doses compared to the reference vertical position at different patient vertical positions starting from 6 cm below and ending at 5.4 cm above the reference level. The effect of a beam-shaping filter appears as the parabolic shape of the dose curves (Study I).

In Study II, clinical chest CT protocols with TCM served to scan three different-sized anthropomorphic phantoms without MOSFET dosimeters. $CTDI_{vol}$ and SSDE values were used to evaluate patient exposure. Using posterior to anterior (PA) scouts for TCM yielded the highest radiation doses when the phantoms were centered at the lowest table-height position, and the lowest when the phantoms were at the highest table-height position (Figure 7). Using lateral (LAT) scouts for TCM yielded smaller changes in radiation doses than using PA scouts did. The relative changes in radiation doses were higher for the adult female phantom than for the two pediatric anthropomorphic phantoms. In the adult phantom, the relative $CTDI_{vol}$ increased as much as 38% over that of the reference position when the phantom was positioned 6 cm below the isocenter, and decreased as much as 23% when the phantom was centered 6 cm above the reference level. Furthermore, the relative changes for the pediatric five-year-old phantom were as much as 21% higher and 12% lower, and for the newborn phantoms, as much as 12% higher and 8% lower.

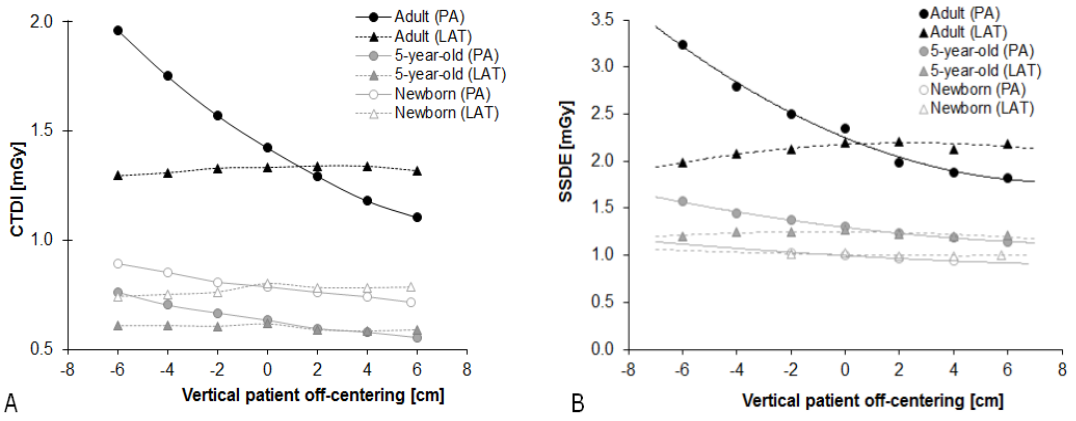

Figure 7 Patient exposure as a function of vertical off-centering of the phantoms from the reference position after using PA and LAT scouts for TCM: **a)** $CTDI_{vol}$, **b)** SSDE. Note that the 16-cm CTDI head phantom served as a reference for the newborn phantom, whereas the 32-cm CTDI body phantom served as the pediatric five-year-old phantom and the adult female phantom (Study II).

According to Study II, the mean image noise was the lowest when the phantoms were properly centered (the axial center of mass) at the scan isocenter and higher when the phantoms were vertically more off-centered from the isocenter (Figure 8). The increase in relative noise was higher for each phantom after using the LAT scout for TCM. Furthermore, using different bowtie filters yielded a greater increase in relative noise for the pediatric phantoms compared to the adult phantom.

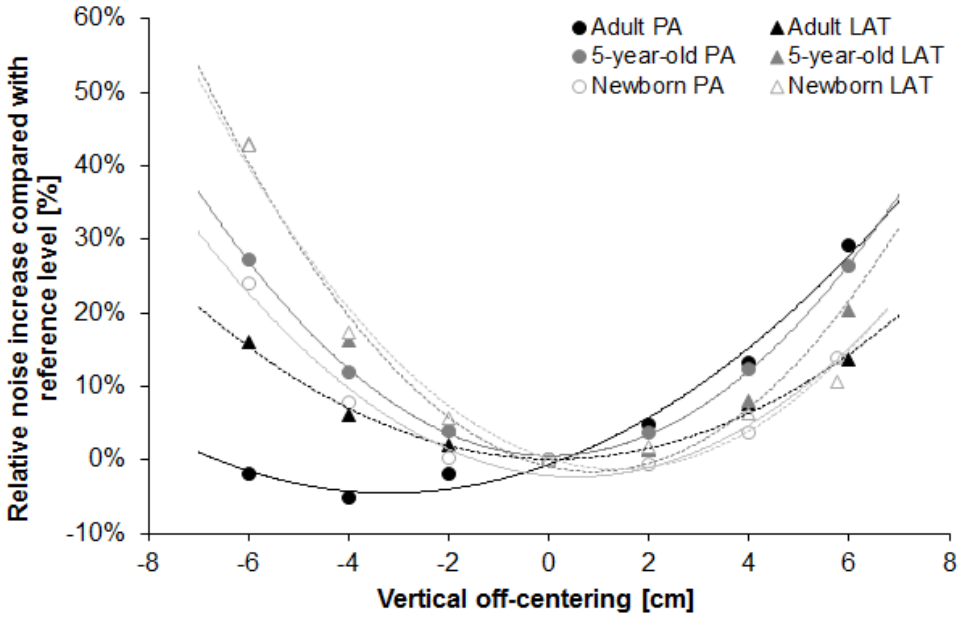

Figure 8 The relative increase in mean noise compared to the reference level as a function of the vertical off-centering of the phantoms. The increase in noise was greater when using LAT scouts for TCM and when centering the phantoms below the isocenter. Image noise was the least when scanning was performed after positioning the phantoms appropriately on the scan isocenter (the center of mass of the phantoms at the isocenter of the CT scanner) (Study II).

4.2 OPTIMIZING CRANIAL CT STUDIES

4.2.1 USE OF MODEL-BASED ITERATIVE RECONSTRUCTION FOR CRANIOSYNOSTOSIS CT

Study III examined the possibilities of using a model-based iterative reconstruction technique to reduce patient doses to ultralow-dose levels in craniosynostosis imaging. The phantom measurement results shown in Figures 9 and 10 reveal that, with VEO MBIR and ultralow-dose protocols, it was possible to reduce mean organ doses by as much as 83% and 88% compared to routine protocols in pediatric newborn and five-year-old anthropomorphic phantoms, respectively, without sacrificing image quality for diagnosis. The simulation results supported the findings with the MOSFET dosimeters. The thyroid gland received the greatest organ dose in the five-year-old phantom, but the lowest in the newborn phantom, which shows the importance of appropriately limiting the scan range. Otherwise, the mandible, simulating the salivary glands, and the eye lenses received the greatest radiation doses; the dose to the breast was insignificant. The standard deviations of the MOSFET measurements ranged from 4% to 10% with higher dose levels and from 10% to 30% with ultralow-dose levels, although the standard deviation of the breast dose varied from 40% to 120% due to low dose absorption. By using the ICRP 103 tissue-weighting factors in simulations, the routine CT protocols for craniosynostosis resulted in approximately 150- and 105-µSv effective doses for the pediatric newborn and five-year-old phantoms, respectively. Similarly, the lowest effective doses with the ultralow-dose protocols (80-kVp and fixed 10-mA tube current) were approximately 23 and 15 µSv for the newborn and five-year-old phantoms, respectively.

The CT numbers of bone tissue were markedly higher in the VEO images than in the ASIR images. The image noise in ultralow-dose VEO images was roughly the same as in the images scanned with routine CT protocols for craniosynostosis (100 kVp, NI = 35 and ASIR30% for newborn patients, and 120 kVp, NI = 35 and ASIR30% for five-year-old patients). Figure 10 shows the image noise results for the five-year-old phantom. The image noise in the bone tissue varied more than did the image noise in the soft tissue due to beam-hardening artifacts.

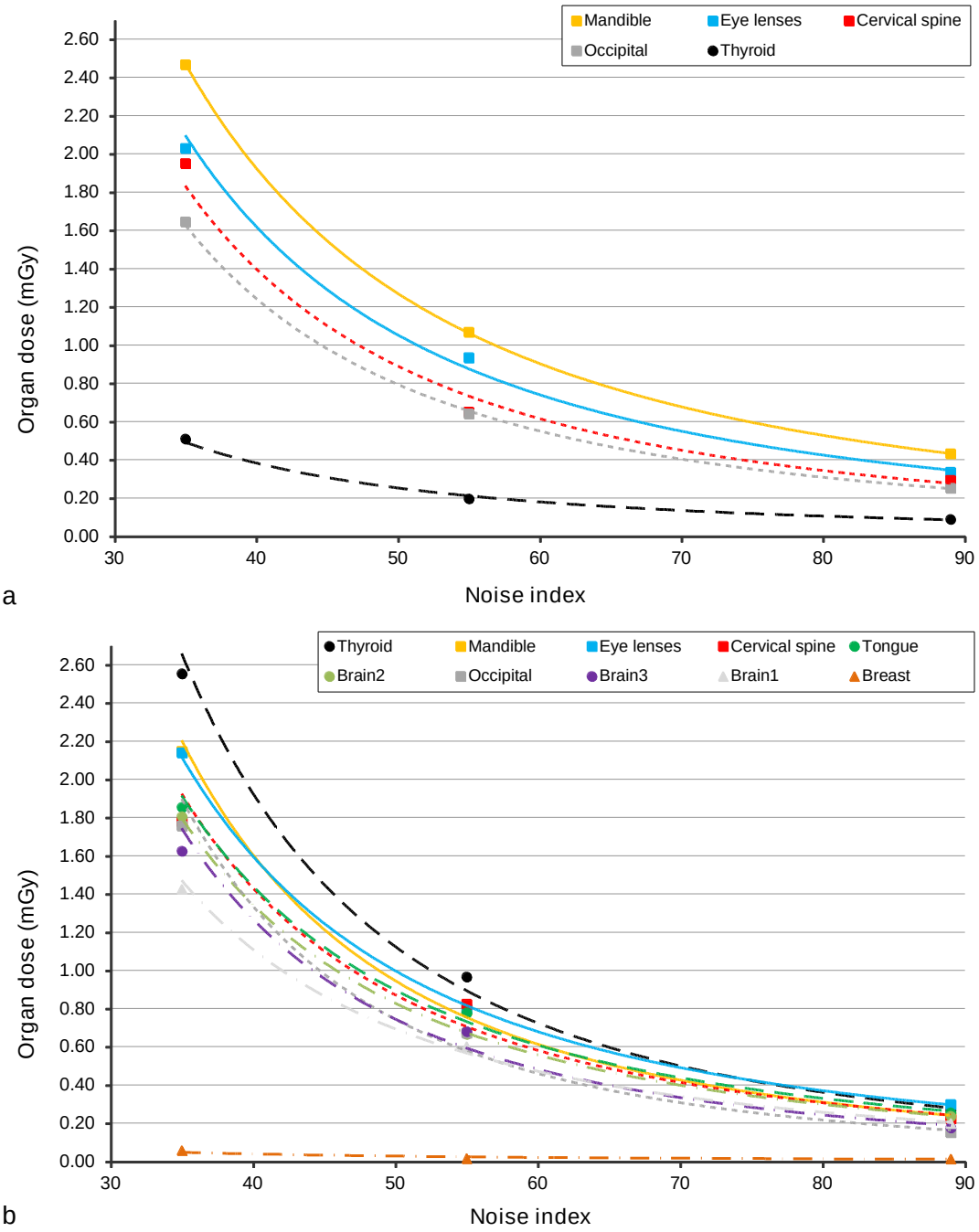

Figure 9 Organ doses measured with MOSFET dosimeters and presented as a function of the applied noise index level. Graph shows organ doses at 80 kVp for (**a**) the newborn and (**b**) five-year-old phantoms. (*Brain 1* is middle line of the frontal lobe at the level of the bulbus; *brain 2* is the right side of the anterior parietal lobe at the middle brain level; *brain 3* is the left side of the frontal lobe at the middle brain level; *occipital* is the posterior middle line of the occipital lobe at the middle brain level). The standard deviations of the measurements ranged from 4% to 10% at higher dose levels and from 10% to 30% at ultralow-dose levels. The standard deviation of the dose to the breast varied from 40% to 120%. Curves indicate the regression model according to the doses measured (Study III).

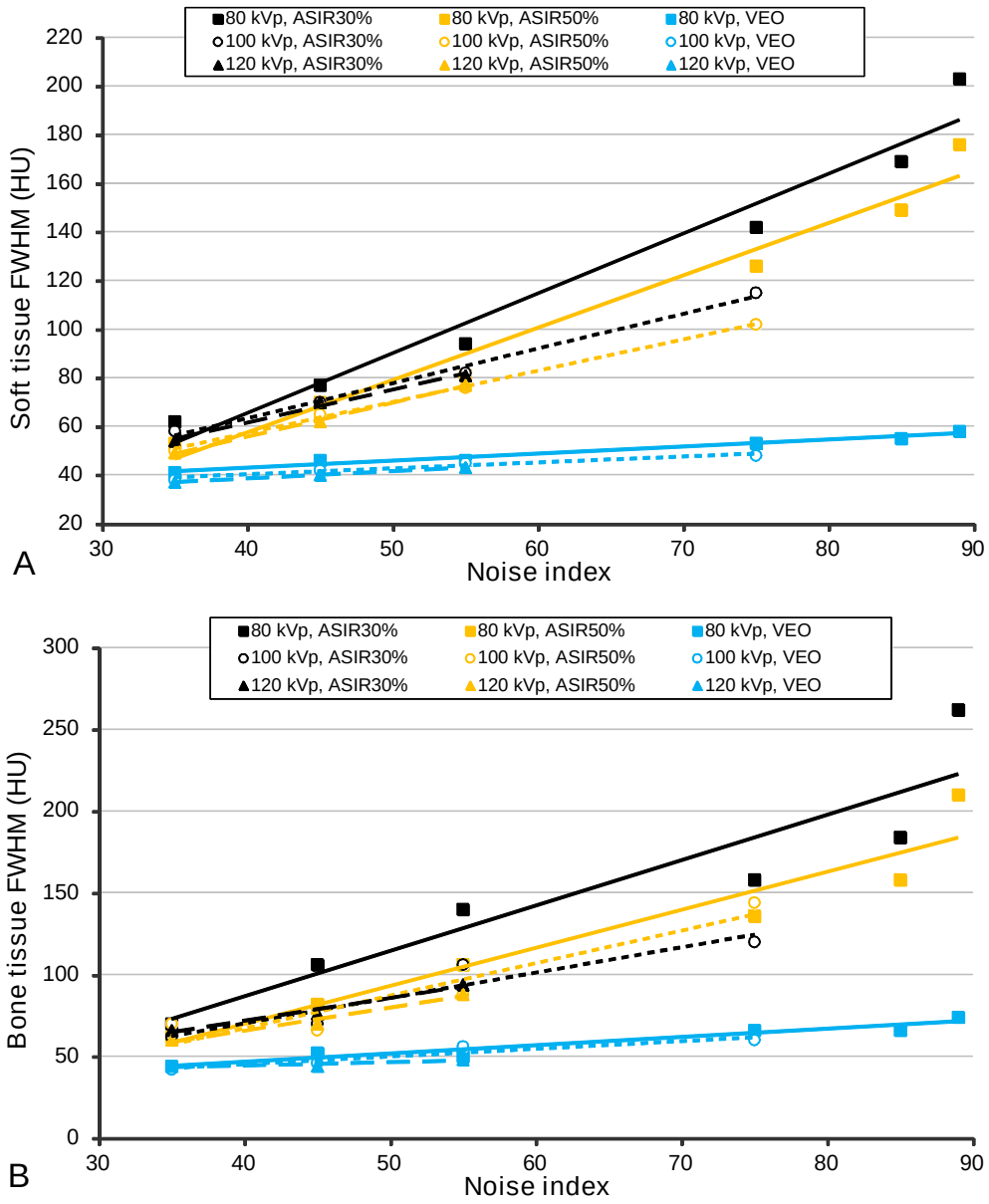

Figure 10 Objective image quality analysis for the five-year-old phantom. The image noise in the soft (**a**) and bone (**b**) tissues, measured as FWHM, increased with higher noise indices. The image noise was approximately the same in VEO reconstruction with the lowest exposure parameters, as in the routine CT protocol for craniosynostosis (Study III).

4.2.2 REDUCING EYE LENS DOSES IN ROUTINE HEAD CT EXAMINATIONS

In Study IV, we used two anthropomorphic head phantoms to study different optimization practices for reducing radiation exposure to the eye lenses. The mean organ doses absorbed in the head region varied from 2.2 to 22.8 mGy for the ATOM phantom, and from 3.1 to 20.9 mGy for the RANDO phantom. Depending on the scan settings, the mean lens dose varied from 4.9 to 19.7 mGy for the ATOM phantom and from 10.8 to 16.9 mGy for the RANDO

phantom. Figure 11 shows the relative absorbed doses to the eye lenses in both phantoms. For the ATOM phantom, using the gantry tilt according to clinical practice in the hospital (baseline set from skull base to radix nasi), with or without bismuth shields, appeared to be the most efficient way to reduce the dose to the eye lenses, decreasing the absorbed dose by approximately 75% from that of the reference setting. Combining OBTCM and gantry tilt reduced the dose by 70%, whereas OBTCM alone reduced the lens dose by only 32%. The 0.06-mm Pb bismuth shield made it possible to reduce the lens dose as much as 25%, whereas the gantry tilt at half the angle used in clinical practice reduced the lens dose by 20% from that of the reference setting. For the RANDO phantom, the dose reduction was less significant and occurred in a different order than for the ATOM phantom due to different phantom geometry. A combination of OBTCM and gantry tilt with the RANDO phantom yielded the greatest reduction in lens dose (36%), whereas gantry tilt alone reduced the dose to the eye lenses by only 18%. In addition to uncertainty with the single MOSFET measurement, the differences between the measured right and left lens doses also stem from the helical scan technique, and with regard to OBTCM, from the boosting of the posterior tube current and the dose gradient of the OBTCM technique that Siemens CT scanners employ.

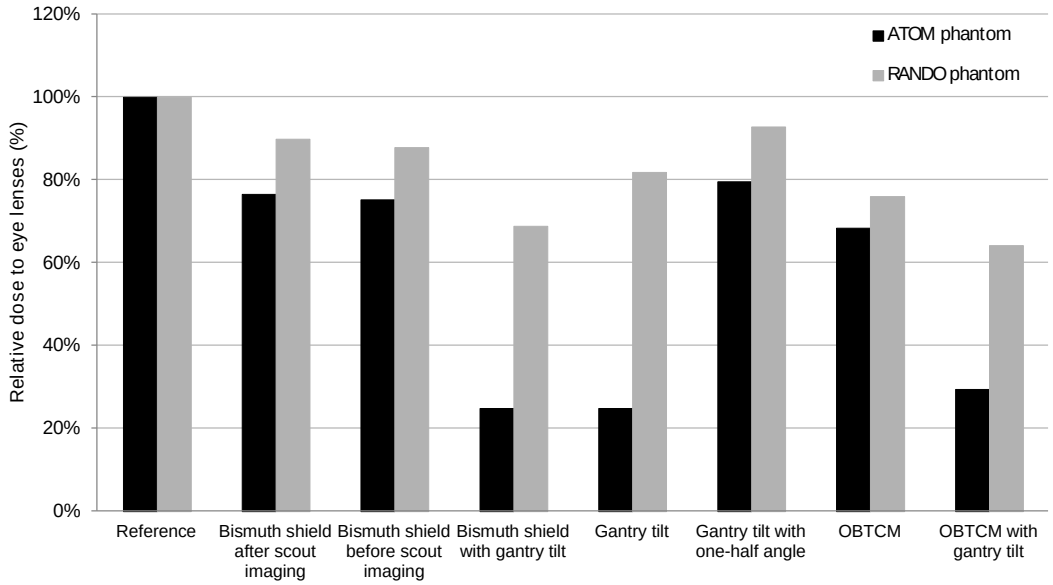

Figure 11 The mean relative absorbed doses to the eye lenses in two anthropomorphic head phantoms. As seen from the graph, the dose reductions achieved over those achieved with the reference scan settings with no optimization methods were minor in the RANDO phantom, which shows the effect of patient geometry on dose-reduction capabilities (Study IV).

The image quality analysis with the ATOM phantom showed that the image contrast depended little on the scan setting. However, the image noise varied from 4.4 to 6.5 HU. Using Safire (Sinogram Affirmed Iterative Reconstruction), level 2, reduced the image noise by approximately 20%. The use of OBTCM with or without gantry tilt increased the image noise in the bottom and posterior

parts of the brain by as much as 30%. Similarly, OBTCM increased image noise in the anterior and central parts of the brain by about 12% and 29%, respectively. The use of gantry tilt reduced image noise in the anterior part of the brain by approximately 25%. In other regions of the brain, however, the change was more moderate. The use of a bismuth shield increased image noise by approximately 17% in the central part of the brain when the shield was set over the eyes after scout imaging. However, setting the bismuth shield incorrectly, before the scouts, increased image noise less, as TCM compensated for the greater X-ray attenuation by raising the mAs.

4.3 FETAL DOSES IN DIFFERENT STAGES OF PREGNANCY IN THE MOST COMMON EMERGENCY CT EXAMINATIONS DURING PREGNANCY

In Study V, we determined fetal doses in different stages of pregnancy and CT indications with an anthropomorphic female phantom and MOSFETs. Because TCM modulated the tube current depending on the patient's size, the mean fetal dose remained fairly constant through all stages of pregnancy in both trauma (4.4-4.9 mGy) and abdominopelvic (2.1-2.4 mGy) protocols (Table 2). In pulmonary angiography, however, the fetal dose decreased exponentially with increases in the distance from the end of the scan range (0.01-0.09 mGy).

The relative doses between the mean $CTDI_{vol}$ and mean fetal dose in different stages of pregnancy ranged from 0.80 to 0.97 for the trauma protocol. Similarly, abdomino-pelvic and pulmonary angiography protocols ranged from 0.57 to 0.79 and from 0.01 to 0.05, respectively.

Table 2 – Mean fetal doses (D_f), corresponding to mean $CTDI_{vol}$ values in mGy and calculated relative doses (mean D_f / mean $CTDI_{vol}$) in three CT scan protocols and four simulated stages of pregnancy (12, 20, 28 and 38 weeks of pregnancy) (Study V).

Protocol	12 weeks	20 weeks	28 weeks	38 weeks
Trauma				
Mean D_f	4.60 (4.21-5.26)	4.87 (4.21-5.59)	4.39 (3.30-5.12)	4.64 (3.45-5.46)
Mean $CTDI_{vol}$	4.74	5.15	5.30	5.79
Relative dose	0.97	0.95	0.83	0.80
Abdomino-pelvic				
Mean D_f	2.06 (1.83-2.51)	2.41 (1.94-3.07)	2.14 (1.62-2.61)	2.21 (1.79-2.71)
Mean $CTDI_{vol}$	2.63	3.04	3.22	3.91
Relative dose	0.78	0.79	0.66	0.57
Pulmonary angiography				
Mean D_f	0.01 (0.008-0.014)	0.03 (0.006-0.12)	0.06 (0.004-0.25)	0.09 (0.011-0.29)
Mean $CTDI_{vol}$	1.34	1.46	1.54	1.97
Relative dose	0.01	0.02	0.04	0.05

5 DISCUSSION

5.1 ANTHROPOMORPHIC PHANTOMS AND MOSFET DOSIMETERS IN CT OPTIMIZATION

Because medical uses for ionizing radiation account for the greatest man-made contribution to overall radiation doses to the population, efforts should focus on reducing patient doses and optimizing scanning procedures. In CT, optimization can be done in many ways, not only through technical solutions, but also through users. First of all, a physician should select a suitable diagnostic imaging method for a particular disease and prefer noninvasive methods and modalities that do not use ionizing radiation. However, when a CT examination is necessary, one should select and use an appropriate scanning protocol for the indication. Furthermore, by centering the patient appropriately on the scan isocenter, the CT operator ensures a basis for an optimized study.

CT protocols can now be tested with anthropomorphic phantoms in more clinical settings before irradiating real patients. Radiation dose levels can therefore be lowered and image quality improved before beginning clinical examinations in new CT systems. When available, anthropomorphic phantoms can serve in user training and for practicing, for example, procedures for cases of trauma. However, these phantoms also widely serve in research due to their numerous benefits. In this thesis, anthropomorphic phantoms served to explore patients' centering on the CT scanner isocenter (Studies I-II), head scanning optimization for craniosynostosis patients (Study III) and routine head CT examinations (Study IV), as well as to evaluate fetal doses in the most common CT examinations during emergency CT for pregnant women (Study V). Anthropomorphic patient models were equipped with MOSFET dosimeters to determine organ doses in all studies except Study II, where only dose-monitoring software and dose indices served to estimate patients' exposure to ionizing radiation. For image quality analysis, Studies I-III used a more advanced ROI analysis method with HU histogram analysis, but Study IV used manual ROI analysis because of the artifacts resulting from the air gaps between the layers of the phantom when using a gantry tilt.

5.1.1 PATIENT CENTERING

Although many educational workshops and situations have recently highlighted the importance of appropriately centering the patient, an evaluation of clinical patient examinations in Study II of this thesis revealed that patient vertical miscentering remains a common problem, as most of the patients scanned were positioned too low with respect to the isocenter of the CT scanner, yielding medium values between 25 and 35 mm. According to phantom measurements from Study II, when using PA scouts for TCM,

miscentering on this scale will increase the radiation dose by as much as 15% while also compromising the image quality. In the LAT direction, patient positioning proved to be more accurate, possibly because the sides of the patient table provide a good reference for a radiographer. Researchers have noted similar phenomena in other studies [Li et al. 2007; Toth et al. et al. 2007; Habibzadeh 2012]. One possible cause of vertical off-centering errors in diagnostic CTs is the shape of the patient table which, unlike the tables of CT simulators used for radiotherapy, is curve-shaped. Consequently, a radiographer may be unaware that the patient will likely to be positioned a few centimeters below what is visible. Patient positioning errors affect the function of TCM systems and may therefore outweigh the benefits of TCM use. Ideally, for optimized TCM function, imaging should take place with the axial center of attenuation of the object on the isocenter. In reality, however, the center of attenuation depends on the z-location and therefore cannot remain at the isocenter for the entire scanning range, and one should use a mean value from the scanning range. Unfortunately, due to differences in the body areas and patients scanned, providing an explicit rule of thumb to visually make a table transfer from optimal geometrical patient centering to optimal patient positioning that takes into account the axial center of attenuation of the object is impossible.

As Studies I-II of this thesis showed, inappropriate patient positioning on the scan isocenter markedly affects both patient dose and image quality, and may lead to insufficient image quality and a repeated scan. Due to the shapes of the beam-shaping filters, the effects of miscentering are most evident in radiosensitive surface tissues (i.e. the breasts, thyroid etc.) and vary between different-sized patients. In Study II, the relative change in $CTDI_{vol}$ or SSDE proved to be higher in larger phantoms after using a PA scout for TCM and when centering the phantoms below the isocenter, by as much as 38%, 21%, and 12% for adult female, pediatric five-year-old and newborn phantoms, respectively. Such an increase in radiation doses in low off-centering and PA scouts used for TCM occurs because the scout image magnifies the projected area of an object, yielding higher mAs for the helical scan [e.g. Matsubara et al. 2009]. The effects of bowtie filters on image noise stems from the parabolic shapes of the mean image noise curves (Figure 8). Changes in image quality occurred not only in image noise, but also in CNR and image contrast values. Study I found that the CT value in, for example, soft tissue may change from 10 HU to 20 HU depending on the patient's vertical centering. Therefore, when ROI analysis is used to measure absolute CT values, such as in the diagnostics of adrenal gland masses where masses of less than 10 HU in unenhanced CT are considered benign adrenal adenoma [Boland et al. 1998], one should view the results with caution. In this thesis, only GE CT scanners were used to study the effect of patient positioning, so dose and image quality results may vary between other systems due to different TCM techniques and bowtie filters used between CT vendors. Siemens and Philips scanners, for example, adjust the tube current based on online feedback (measurements

from previous 180º views), whereas GE and Toshiba systems perform a predictive calculation or sinusoidal interpolation between PA and LAT scout views [Kalra et al. 2004b].

To overcome the patient centering problem, patient positioning should be included as an important part of user training and further discussed in various radiological meetings. When scanning body areas including the spine and lungs, patient's vertical centering on the isocenter becomes more challenging due to a greater asymmetry in net attenuation in the AP/PA direction compared to the SIN/DEX direction. Therefore, to position the patient more accurately on the isocenter, scout imaging should also be done in the LAT direction in addition to the PA direction. However, in ultralow-dose scans, such as those used in protocols constructed for craniosynostosis (Study III), using two scouts may expose the patient to a significantly higher radiation dose than with a primary scan [Schmidt et al. 2013]. When TCM is used in chest CT with CT scanners manufactured by GE, the use of a LAT scout as the last scout projection yields more stable patient dose levels than when the PA scout is the last projection if the patient vertical centering varies. In such cases, however, the image quality will suffer. To position patients on the center of the attenuation axis and to overcome the miscentering problem, CT manufacturers could potentially develop more effective tools that would automatically correct the patient vertical positioning with a LAT scout. A current solution to the patient miscentering problem with some CT scanners from Toshiba only detects the offset between the patient position and the gantry isocenter, and then tries to adjust the tube current as the patient was on the isocenter. As a result, the dose absorbed by the patient may be lower, but the image quality will likely be suffered as a result of the beam-shaping filters because the patient is still off the isocenter. Therefore, to obtain the most optimal results, both in terms of image quality and radiation dose, one should also correct the patient positioning after the scout and not only to adjust the tube current. Additionally, the use of dose-monitoring software (as in Study II) may be helpful for improving imaging practices because such software provides immediate feedback from the scans, including patient's centering. Dose-monitoring software can also serve to manage CT doses on a larger scale and provide helpful tools for optimization and managing, especially for physicists.

5.1.2 OPTIMIZING CRANIAL CT STUDIES

Of all the areas of CT imaging, head CT examinations are the most common [Helasvuo 2013]. In addition, CT scans of the cranial bones are one of the most common CT examinations among children. In this thesis, two publications (Studies III-IV) explored the optimization of head CT examinations; Study III focused on craniosynostosis imaging, whereas Study IV focused on the optimization of routine head CT studies, and especially on reducing radiation exposure to the eye lenses.

Several optimization methods can serve to reduce the radiation dose to the eye lenses [e.g. Hopper et al. 2001; Heaney et al. 2006; Reimann et al. 2012; Wang et al. 2012a], and thereby also minimize cataract risk. As Study IV showed, the most effective method for reducing doses was gantry tilting, which, in the ATOM phantom, reduced the dose to the eye lenses by as much as 75%. However, patient geometry may yield significant differences in dose reduction capabilities, as we observed with the two phantoms. With the RANDO phantom, gantry tilt alone reduced the eye lens dose by only one fifth, showing the effect of allowing the lenses to remain partly inside the primary beam. Although gantry tilting angles between patients can vary markedly in routine work due to patient-specific physiological limitations, even a small tilting angle proved useful, as it shortened the scanning range and thereby reduced the total radiation dose. Because some CT scanners do not permit gantry tilting, users can mimic gantry tilt by placing the patient's head on a head support with the chin tucked down to the chest. However, tilting the patient's head is not always possible for anatomical reasons and due to the patient's physiology. In such cases, the use of bismuth shields or OBTCM can be considered the primary means to minimize the dose to the eye lenses. Interestingly, however, the use of OBTCM appeared to increase image noise in the posterior and central parts of the brain, whereas using bismuth shields over the eyes proved advantageous while only slightly compromising the image quality of brain scans. OBTCM techniques differ between vendors, so the results achieved with a Siemens CT scanner in Study IV may differ from results with Toshiba and GE scanners, which do not boost the tube current from the posterior side and use different angles to reduce the tube current during tube rotation.

Besides attempting to reduce the eye lens doses in routine head CT examinations, CT optimization in the head region, such as in craniosynostosis imaging, studied in publication III, has specific needs. CT as a diagnostic tool for diagnosing and following the treatment of craniosynostosis may expose children who frequently undergo repeated CT examinations at the time of diagnosis and at various stages of surgical corrections to a relatively high radiation dose. The effective dose of a routine head CT typically varies from about 0.5 to 2 mSv. However, because the inherent contrast between the skull and soft tissue is higher than between the cranial soft tissues, a CT examination of the skull can be performed with less radiation. The ultralow-dose CT protocols developed in Study III enable one to reduce the patient dose by about 85% compared to routine scanning protocols for craniosynostosis used in the hospital without compromising diagnostic image quality. Clinically acceptable image quality was achievable with CT protocols resulting in an approximately 20-µSv effective dose for the patient, which is up to 100 times lower than the dose in standard head CT for the brain, and far below the 0.2 to 2.8 mSv previously reported for craniosynostosis CT imaging [Cerovac et al. 2002; Jaffurs and Denny 2009; Didier et al. 2010; Vazquez et al. 2013; Calandrelli et al. 2014], although in a very recent publication, MBIR

resulted in sufficient image quality for craniosynostosis with $CTDI_{vol}$ values comparable to those in Study III of this thesis [Widmann et al. 2015]. Additionally, the dose achieved in Study III of this thesis corresponds to the effective dose in plain skull radiography, which falls between 0.01 and 0.04 mSv [Cerovac et al. 2002; Jaffurs and Denny 2009]. As the dose measurements and numerical simulatios results showed, appropriately limiting the scan range is important in reducing doses to the thyroid and salivary glands.

The image quality of low-dose craniosynostosis CT examinations that use the VEO reconstruction technique were superior to ASIR images with either 30% or 50% blending levels of ASIR-FBP. Specifically, VEO MBIR images had significantly less image noise than did ASIR images, although the image matrix in VEO was higher, resulting in smaller voxels, which theoretically results in relatively higher image noise than with larger image voxels. To understand the huge difference between these techniques, we obtained ultralow-dose images with VEO using similar image noise levels to those in routine CT protocols that use ASIR30%. The bone tissue contrast was markedly higher with VEO, which may stem from the capability of VEO to suppress the beam hardening and streaking artifacts caused by the skull bones. Thus, VEO may quantify the CT numbers of bone tissues more accurately than ASIR does. However, this difference in CT numbers between reconstructions requires more thorough study.

Although the use of VEO showed substantial benefits, its use in clinical applications, and especially in acute examinations, is limited by long reconstruction times. Despite the availability of advanced server technology, current reconstruction times range from 15 to 90 minutes. However, because CT scans for craniosynostosis are non-emergency examinations, long reconstruction times are not critical, so VEO could prove suitable in patients requiring repeated scans throughout their life. Although not yet available, the ultralow-dose craniosynostosis CT protocols currently under development will serve in patient scanning in the near future, and future studies will evaluate their clinical feasibility more accurately. Another limitation of VEO is that it can only be used in some of the newest GE CT scanners. However, all CT manufacturers nowadays offer their own iterative reconstruction techniques, though usually not a model-based iterative reconstruction.

5.1.3 FETAL DOSE IN CT SCANS OF PREGNANT WOMEN

Occasionally, the CT examination of a childbearing mother is needed when other diagnostic tools are insufficient, and the life of the mother or unborn child is threatened [Goldberg-Stein et al. 2011]. Such cases usually require estimates of the fetal dose and its risks to the development of the unborn child. The dose absorbed by the uterus has served as a surrogate for the dose absorbed by the embryo and fetus in medical radiation dosimetry [ACR 2013]. According to previous studies, the fetal dose can typically be estimated from

the uterus dose with a precision of about 15%-20% [Felmlee et al. 1990; Damilakis et al. 2000]. Based on the fetal radiation dose levels measured in Study V (less than 5 mSv in all CT indications studied), the radiation dose to the fetus poses no obstacle to an optimized CT examination with a medically necessary indication. Other CT publications have drawn similar conclusions [Helmrot et al 2007; Jaffe et al. 2008]. Moreover, the radiation dose resulting from a single CT scan causes no tissue reactions in the fetus, but may become a concern with multiple exams. Additionally to our fetal dose CT study, Manninen et al. (2014b) used RPLDs to study the fetal radiation doses in fluoroscopy during prophylactic catheterization and uterine artery embolization. According to their study, the mean estimated fetal dose (vaginal dose *in vivo*) of seven patients was 11.2 ± 9.1 mSv. Thus, the mean absorbed dose of that fluoroscopic procedure was about five times higher than the dose measured in Study V of this thesis for an abdomino-pelvic CT examination.

When the fetus is entirely in the primary scan range, the fetal dose estimation can be based on console $CTDI_{vol}$ values (the annual tests confirmed the accuracy of the dose display), which work as an upper estimate of the fetal dose. If the fetus is outside of the primary scan range, the fetal dose is mainly a function of the distance from the scan range due to the level of scattered dose contribution. As Study V shows, the fetal dose dropped quickly as the distance from the scan range increased. According to the results, when the fetus is more than 20 cm from the caudal end of the scan range, the fetal dose in early pregnancy is very low. However, as the fetus grows and the uterus extends more cranially, the dose to the fetus increases exponentially ($D_f = 4.6953e^{-0.2629x}$) as distance x from the scan range decreases. Although the fetal dose in chest CT examinations may be particularly low, a recent publication has proposed using bismuth shields in these scans, resulting in substantial dose reduction [Chatterson et al. 2014].

It is worth remembering that the dose to the uterus does not represent the fetal dose, as its size and position depends on the gestational age. This seems obvious, but it also means that standard mathematical phantoms should not be used to calculate fetal doses. Various methods have been used to estimate the fetal volume during pregnancy, but, more importantly, could instead serve to estimate the fetal position, namely whether the fetus is partly or wholly in the radiation beam or in the vicinity of it. The uncertainties of the fetal dose are therefore two-dimensional: in early stages of pregnancy, the fetus's organs and tissues will likely be exposed to equivalent doses, but the place of fetus in the uterus may vary; in later stages of pregnancy, the position of the fetus in the uterus may vary, and different organs and tissues may no longer be exposed to the same doses. The following chapter of this thesis will discuss more about the uncertainties related to patient dose measurements.

5.2 UNCERTAINTIES RELATED TO PATIENT DOSE MEASUREMENTS

Certain uncertainties relating to patient dosimetry should be taken into account, especially when determining organ doses and effective doses. Although the effective dose should not be used to assess individual risk, but only to describe the increased health risk for the population at large, it is a practical dose quantity used to optimize radiological examinations that can link physically measurable dose quantities and the risk for health detriment. Specifically, the effective dose can serve to compare radiation doses from different radiological techniques and imaging methods with respect to stochastic health detriment [ICRP 2007]. Although very usable, determining the effective dose can be problematic. The tissue-weighting factors used to calculate effective doses are based on atomic bomb data with whole-body irradiations, which is problematic in diagnostic imaging as organs and tissues receive only partial or very heterogeneous exposure. Additionally, the effective dose is determined for workers and the general population, which can have an age distribution different from the age distribution of patients undergoing medical procedures using ionizing radiation [ICRP 2007]. The risk for different age groups (e.g. children and the elderly) may vary by a factor of four to five [Preston et al. 2007]. In this thesis, effective doses were determined only in Study III by using simulations. In Studies I and III-V, we used MOSFET dosimeters and anthropomorphic phantoms to determine organ doses. The uncertainties of dosimetric calculations with dosimeters fall into two categories of uncertainty [IAEA 2005; IAEA 2007]: type A, which is a standard deviation of the single dosimeter readings (thus, reflecting the reproducibility of each measurement), and type B, which takes into account all physical uncertainties, including uncertainties relating to, for example, positioning of the phantoms and dosimeters, X-ray spectra and beam intensity, and the angular dependency of dosimeters. For example, the estimated type B uncertainty of a single MOSFET measurement in Study V was 5%, whereas the estimated mean total uncertainty (type A and B) of a single MOSFET measurement was 7%-11%. Moreover, when determining the dose absorbed by each organ, as well as the effective dose, one should take into account the fraction of irradiated tissue [e.g. Koivisto et al. 2012; Koivisto et al. 2013a; Manninen 2014a]. Typically, the overall uncertainties in effective dose estimations for a reference patient range from 15% to 40% [Martin 2007; Gregory et al. 2009]. However, when considering the individual's dose from the medical examination, differences in age, gender and mass may lead to additional variations [Martin 2007].

5.2.1 UNCERTAINTIES WITH MOSFET DOSIMETERS

Using MOSFET dosimeters with anthropomorphic phantoms proved suitable for dose assessments in all the studies in this thesis. However, as previously noted, the use of MOSFETs in low-dose X-ray examinations may be limited,

as measuring doses with less than 25% uncertainty at the 95% confidence level requires an absorbed dose of more than 1.4 mGy for high-sensitivity and of 4 mGy for standard-sensitivity MOSFETs [Peet and Pryor 1999; Yoshizumi et al. 2007]. Similarly, Koivisto et al. (2015) observed a single MOSFET low-dose exposure limit of 1.69 mGy for 25% measurement uncertainty at the 95% confidence level. Their other studies saw greater uncertainty with lower doses [Koivisto et al. 2012, Koivisto et al. 2013a]. The low-dose detection limit of RPLDs was 20 µGy with a coefficient of variation of 12.2% [Manninen 2014a]. Additionally, TLDs can also be used for low-dose measurements, as LiF (Mg, Cu, P) TLDs, for example, have a linear dose response from 1 µGy to 10 Gy [IAEA 2007]. Koivisto et al. (2015) found that attaining the corresponding TLD low-dose limit of 0.3 mGy required an average of eight MOSFET exposures. Thus, the sensitivity of MOSFETs is lower than that of both TLDs and RPLDs. Hardening the beam also decreases MOSFET sensitivity, as the PMMA and free-in-air measurements by Koivisto et al. also show (2013b).

In this thesis, the type A uncertainties caused by low absorbed doses decreased and reproducibility increased either by performing several irradiations before reading the MOSFETs, and then dividing the reading results by the number of irradiations, or by using higher dose levels, either by using a fixed mAs or reducing the noise index used for scanning, and then normalizing the results. As anticipated, however, the percentage SD increased as the dose to a MOSFET decreased. For example, the irradiation events with the ultralow-dose protocols used for craniosynostosis (Study III) had to be performed five times before reading the MOSFETs, which resulted in a cumulative $CTDI_{vol}$ of 1.1 mGy. Moreover, the uncertainties of fetal dose estimations were greater in pulmonary angiography than in abdomino-pelvic and trauma scans, as the fetus was outside the primary beam (Study V).

Some other points should also be taken into account when using MOSFET dosimeters in CT. Single MOSFET readings may fluctuate because the CT helical beam does not fall on the same organ location at the same point of the arc due to differences in the X-ray tube start angle between measurements. To overcome this problem, we performed several irradiations before reading the MOSFETs. Additionally, the energy response of the MOSFET dosimeters varies somewhat over the range of energies used in CT [Ehringfeld et al. 2005], although Koivisto et al. (2015) reported a statistically insignificant energy dependency of the current MOSFETs in the energy ranges (50-90 kVp) used in dental cone-beam CT. Therefore, a calibration of the dosimeters at each energy level used for a particular examination is essential prior to taking measurements. Another limitation of MOSFET dosimeters is the finite lifetime of dosimeters in terms of accumulated voltage. For example, the lifetime of MOSFETs used in this thesis accumulated a threshold voltage of 20 000 mV corresponding to an absorbed radiation dose of 7.4 Gy at the high-bias setting (2.7 mV/cGy) and 20 Gy at the standard-bias setting (1 mV/cGy). Moreover, researchers have reported a 1% decrease in sensitivity per 1 000 mV for accumulated threshold voltages between 8 300 mV and 17 500 mV for

the MOSFETs also used in this thesis [Koivisto et al. 2015]. In addition, Brady and Kaufman (2012) observed a 1% decrease in sensitivity per 1 000 mV of accumulated threshold voltages and determined the calibration precision to be about 5% at the dose levels also used in this thesis for MOSFET calibration. MOSFET dosimeters have also shown a significant angular dependency that is considerably smaller in soft tissue material than in free-in-air measurements (up to 30%-40% in normal-to-axial and tangent-to-axial rotations) due to the smoothing effect of the scattered radiation in the material [Pomije et al. 2001; Dong et al. 2002; Roschau and Hinterlang 2003; Ehringfeld et al. 2005; Koivisto et al. 2013b]. However, angular dependences become more important if MOSFETs are placed near bone surfaces. In addition to MOSFETs, other dosimeters may have also significant angular dependences; RPLDs with a tin filter, for example, showed a nearly 50% difference in the measured dose [Manninen 2014a]. According to specifications of the MOSFETs used in this thesis, the inherent build-up depth is 0.8 mm, which provides flexibility in measuring a surface dose as well as the dose at the dose maximum. Additionally, manufacturer of the used MOSFETs guarantee them to be both temperature and dose-rate independent. The literature also contains reports of dose and dose-rate sensitivity independence [Koivisto et al. 2015]. Finally, the MOSFET cables also create uncertainty, but only of about 1% [Ehringfeld et al. 2005].

Dose measurements performed with MOSFET dosimeters, as well as with all other dosimeters, are always point-measurements with a limited number of dosimeters placed into the limited number of organs and tissues. Therefore, the organ and effective dose assessments are also somewhat limited. For example, in Study I of this thesis, the lung tissue dose was determined with five dosimeters, the liver dose with four dosimeters, and the kidney dose with one dosimeter. Due to steep dose gradients at the limits of the scan range, the uncertainties of organ dose assessments are higher when determining organ doses that are either wholly or partly outside the primary beam. For example, in Study I, parts of the liver lay both in and outside the primary beam, resulting in an estimated total uncertainty of the liver dose as high as 50-100%. To overcome the point-measurement limitation with MOSFETs, MOSFET measurements can also work in combination with Monte Carlo simulations by using either a standardized mathematical phantom or, more realistically, the image data from the anthropomorphic phantom. Future studies may aim to use MOSFET dosimeters to verify the results of voxel-based Monte Carlo simulations from the image data. However, voxel-based Monte Carlo simulations were not used in this thesis. In Study III, we evaluated both the organ doses with MOSFET dosimeters and simulations with mathematical phantoms. The results were fairly similar in the primary scanning range, whereas the peripheral areas and areas outside the scanning range revealed more deviation, which partly showed the sensitivity problems with MOSFETs at low-dose levels, and the limitations of using simple mathematical phantoms in simulations. The voxel-based Monte Carlo simulations have

agreed closely with the values measured under both the simple and complex geometries, including an anthropomorphic phantom [Bostani et al. 2014]. These simulations have also agreed closely with doses measured *in-vivo* using TLDs in patients undergoing a virtual colonoscopy [Bostani et al. 2015b].

5.2.2 UNCERTAINTY FROM OTHER SOURCES

Because patient and organ sizes and geometries, as well as organ locations inside the human body vary among patients, the value of a single anthropomorphic phantom in dose assessment is limited. Anthropomorphic phantoms, with limited numbers of averaged anatomical structures, are at best coarse estimations of real patients. For example, different soft tissues inside the phantoms are averaged in their attenuation properties, which yield similar attenuation values for all soft tissues. However, because the attenuation properties of tissues in real patients also varies, the HU values measured in anthropomorphic phantoms correspond well with the mean HU values measured in real patients [Winslow et al. 2009]. Another limitation of commercial anthropomorphic phantoms is that they are often limited to a single reference size in each age group, which often may not be representative of the patient population at large. Therefore, some have recommended using custom-made phantoms with additional adipose tissue-equivalent materials [Fisher and Hintenlang 2014]. Additionally, scan ranges set by radiographers may vary substantially and cause uncertainty in patient dose estimations in clinical environments. To determine organ doses from a CT scan for a particular patient, one should use Monte Carlo simulations that employ CT image data and specific scanner information [e.g. Bostani et al. 2015b]. In the future, CT manufacturers could perhaps accomplish this by building fast Monte Carlo simulation-based calculation software into their scanners.

Other sources that cause uncertainty in patient dose estimations include CT scanners themselves. Since focus-detector and focus-isocenter distances, TCM techniques, beam-shaping filters and iterative reconstruction techniques all vary between vendors and their scanners, the effects of parameter changes on patient dose will differ between scanners. However, even though patient dosimetry with MOSFET measurements and anthropomorphic phantoms contains uncertainty, such equipments are exceptionally useful in CT optimization, and their use should be encouraged.

6 CONCLUSIONS

Despite the technical innovations developed by CT vendors, the role of users in CT optimization remains important. In this thesis, anthropomorphic phantoms and MOSFET dosimeters proved to be feasible and excellent tools in dose assessment and CT optimization, even with ultralow-dose CT protocols to determine the radiation exposures to patients undergoing craniosynostosis imaging. Additionally, the semiautomatic image quality analysis based on HU histograms used in Studies I-III proved applicable for comprehensive and user-independent evaluations of image noise and contrast. This thesis clearly shows that vertically off-centering patient remains a common and serious problem in chest CT regardless of patient size, and that educational meetings for radiographers in particular should focus on this important subject. It seems that a majority of scanned patients are positioned below the isocenter of the CT scanner, resulting in variations in both radiation doses and image quality, measured as image noise, contrast and CNR. Centering the patient vertically below the isocenter of the CT scanner and using a PA scout for TCM can significantly increase the radiation dose and expose anterior radiosensitive surface tissues in particular to greater risks for radiation-induced health detriments due to the non-optimal functioning of beam-shaping filters. Moreover, because the typical offset for small patients (i.e. pediatric patients) was greater than for larger patients, special attention should focus on correctly centering the patient when preparing pediatric patients for CT scans.

As a part of this thesis, we developed ultralow-dose CT protocols that use a model-based iterative reconstruction for craniosynostosis imaging and found that craniosynostosis CT imaging could be performed for the patient with an effective dose of approximately 20 μSv without compromising diagnostic image quality. This dose is comparable to the radiation exposure of plain skull radiography and is more than 80% less than that produced by routine CT protocols used in the hospital for craniosynostosis. Additionally, we found that when in the primary beam, the MOSFET dosimeters yielded results in the head region comparable to the numerical simulations.

In routine head CT, the gantry tilt appears to be the most efficient way to reduce the radiation dose to the eye lenses, as it resulted in as much as a 75% decrease in the dose to the lenses while preserving the image contrast and reducing the image noise, especially in the anterior part of the brain. Because not all CT scanners permit gantry tilting, and because the eye lenses of all the patients cannot be fully excluded from the exposed scan range, OBTCM or bismuth shields can also serve, with some caution, to reduce the exposure of the lenses to radiation.

Because pregnant women sometimes require a CT scan, the simple practices for estimating fetal dose are useful. This thesis shows that when the

fetus lies entirely in the primary scan range, the $CTDI_{vol}$ value from the scanner console serves as an upper estimate of the fetal dose. However, if the fetus lies outside the primary scan range, the fetal dose is mainly a function of the distance from the scan range thanks to the scattered dose contribution. Based on the absorbed radiation dose levels measured in this thesis, the radiation dose to the fetus poses no obstacle to an optimized CT examination with a medically necessary indication.

REFERENCES

American Association of Physicists in Medicine (AAPM). AAPM Report no. 204: Size-specific dose estimates (SSDE) in pediatric and adult body CT examinations. Report of Task Group #204 – Computer Tomography Subcommittee. College Park, MD: AAPM 2011.

American College of Radiology (ACR). ACR-SPR practice guideline for imaging pregnant or potentially pregnant adolescents and women with ionizing radiation. In: Resolution 48: ACR 2013 (Revised):1-19.

Aroua A, Trueb P, Vader JP, Valley JF, Verdun FR. Exposure of the Swiss population by radiodiagnostics: 2003 Review. Health Phys 2007;92:442-448.

Aschan C. Applicability of thermoluminescent dosimeters in x-ray organ dose determination and in the dosimetry of systemic and boron neutron capture radiotherapy. Report series in physics, HU-P-D77. Helsinki: University of Helsinki; 1999. http://urn.fi/URN:ISBN:951-45-8686-7

Attix FH. Introduction to radiological physics and radiation dosimetry. John Wiley, New York, USA 1986.

BEIR (Committee on the biological effects of ionizing radiations). Health risks from exposure to low levels of ionizing radiation: BEIR VII – Phase 2. National Research Council of the National Academies. Washington DC: The National Academies Press 2006.

Beister M, Kolditz D, Kalender W. Iterative reconstruction in X-ray CT. Physica Medica 2012;28:94-108.

Berrington de González A, Mahesh M, Kim KP, Bhargavan M, Lewis R, Mettler F, Land C. Projected cancer risks from computed tomography scans performed in the United States in 2007. Arch Intern Med 2009;169:2071–2077.

Bly R, Järvinen H, Korpela MH, Tenkanen-Rautakoski P, Mäkinen A. Estimated collective effective dose to the population from X-ray and nuclear medicine examinations in Finland. Radiat Prot Dosimetry 2011;147:233-236.

Boland GWL, Lee MJ, Gazelle SG, Halpern EF, McNicholas MM, Mueller PR. Characterization of adrenal masses using unenhanced CT: an analysis of the CT literature. AJR 1998;171:201-204.

Bostani M, McMillan K, DeMarco JJ, Cagnon CH, McNitt-Gray MF. Validation of a Monte Carlo model used for simulating tube current modulation in computed tomography over a wide range of phantom conditions/challenges. Med Phys 2014;41:1-10.

Bostani M, McMillan K, Lu P, Kim HJ, Cagnon CH, DeMarco JJ, McNitt-Gray MF. Attenuation-based size metric for estimating organ dose to patients undergoing tube current modulated CT exams. Med Phys 2015a;42:958-968.

Bostani M, Mueller JW, McMillan K, Cody DD, Cagnon CH, DeMarco JJ, McNitt-Gray MF. Accuracy of Monte Carlo simulations compared to *in-vivo* MDCT dosimetry. Med Phys 2015b;42:1080-1086.

Brady SL, Kaufman RA. Establishing a standard calibration methodology for MOSFET detectors in computed tomography dosimetry. Med Phys 2012;39:3031-3040.

Brenner DJ, Elliston C, Hall EJ, Berdon W. Estimated risks of radiation-induced fatal cancer from pediatric CT. AJR 2001;176:289-296.

Brenner DJ, Hall EJ. Computed tomography-An increasing source of radiation exposure. N Engl J Med 2007;357:2277–2284.

Brix G, Lechel U, Veit R, Truckenbrodt R, Stamm G, Coppenrath EM, Griebel J, Nagel HD. Assessment of a theoretical formalism for dose estimation in CT: an anthropomorphic phantom study. Eur Radiol 2004;14:1275-1284.

Børretzen I, Lysdahl KB, Olerud HM. Diagnostic radiology in Norway – trends in examination frequency and collective effective dose. Radiat Prot Dosimetry 2007;124:339-347.

Calandrelli R, A'Apolito G, Gaudino S, Sciandra MC, Caldarelli M, Colosimo C. Identification of skull base sutures and craniofacial anomalies in children with craniosynostosis: utility of multidetector CT. Radiol Med 2014;199:694-704.

Cameron JR, Suntharalingam N, Kenney GN. Thermoluminescent dosimetry. Madison: University of Wisconsin Press 1968.

Cerovac S, Neil-Dwyer JG, Rich P, Jones BM, Hayward RD. Are routine preoperative CT scans necessary in the management of single suture craniosynostosis? Br J of Neurosurg 2002;16:348-354.

Chatterson LC, Leswick DA, Fladeland DA, Hunt MM, Webster S, Lim H. Fetal shielding combined with state of the art CT dose reduction strategies during maternal chest CT. EJR 2014;83:1199-1204.

Damilakis J, Perisinakis K, Voloudaki A, Gourtsoyiannis N. Estimation of fetal radiation dose computed tomography scanning in late pregnancy. Invest Radiol 2000;35:527-533.

Deak PD, Langner O, Lell M, Kalender WA. Effects of adaptive section collimation on patient radiation dose in multisection spiral CT. Radiology 2009;252:140-147.

Deak PD, Smal Y, Kalender WA. Multisection CT protocols: Sex and age-specific conversion factors used to determine effective dose from dose-length product. Radiology 2010;257:158-166.

Deák Z, Grimm JM, Treitl M. Filtered back projection, adaptive statistical iterative reconstruction, and a model-based iterative reconstruction in abdominal CT: an experimental clinical study. Radiology 2013;266:197-206.

Didier RA, Kuang AA, Schwartz DL, Selden NR, Stevens DM, Bardo DME. Decreasing the effective radiation dose in pediatric craniofacial CT by changing head position. Pediatr Radiol 2010;40:1910-1917.

Ding A, Mille MM, Liu T, Caracappa PF, Xu XG. Extension of RPI-adult male and female computational phantoms to obese patients and a Monte Carlo study of the effect on CT imaging dose. Phys Med Biol 2012;57:2441-2459.

Dong SL, Chu TC, Lan GY, Wu TH, Lin YC, Lee JS. Characterization of high-sensitivity metal oxide semiconductor field effect transistor dosimeters system and LiF:Mg,Cu,P thermoluminescence dosimeters for use in diagnostic radiology. Appl Radiat Isot 2002;57:883-891.

Dougeni E, Faulkner K, Panayiotakis G. A review of patient dose and optimisation methods in adult and paediatric CT scanning. EJR 2012;81:e665-e683.

Duan X, Wang J, Christner J, Leng S, Grant KL, McCollough GH. Dose reduction to anterior surfaces with organ-based tube current modulation: evaluation of performance in a phantom study. AJR 2011;197:689-695.

Ehringenfeld C, Schmid S, Poljanc K, Kirisits C, Aiginger H, Georg D. Application of commercial MOSFET detectors for *in vivo* dosimetry in the therapeutic x-ray range from 80 kV to 250 kV. Phys Med Biol 2005;50:289-303.

European Commission (EC). Study on European population doses from medical exposure (Dose DataMed 2). DDM2 Project report on European population dose estimation. 2013.
http://ddmed.eu/_media/news:ddm2_project_report_population_dose_estimation_final_draft_for_web_page_28_jan_2013.pdf.

FDA - U.S. Food and Drug Administration. Safety investigation of CT brain perfusion scans: Update 11/9/2010. Accessed 29.5.2015.

Felmlee JP, Gray JE, Leetzow ML, Price JC. Estimated fetal dose from multislice CT studies. AJR 1990;154:185-190.

Fisher RF, Hintenlang DE. Super-size me: adipose tissue-equivalent additions for anthropomorphic phantoms. J Appl Clinical Med Physics 2014;15:306-312.

Gies M, Kalender WA, Wolf H, Suess C. Dose reduction in CT by anatomically adapted tube current modulation. I. Simulation studies. Med Phys 1999; 26:2235-2247.

Goldberg-Stein S, Liu B, Hahn PF, Lee SI. Body CT during pregnancy: utilization trends, examination indications, and fetal radiation doses. AJR 2011;196:146-151.

Greffier J, Macri F, Larbi A, Fernandez A, Khasanova E, Pereira F, Mekkaoui C, Beregi JP. Dose reduction with iterative reconstruction: optimization of CT protocols in clinical practice. Diagn Interv Imaging 2015;96:477-486.

Gregory KJ, Bibbo G, Pattison JE. Uncertainties in effective dose estimates of adult CT head scans: the effect of head size. Med Phys 2009;36:4121-4125.

Gu J, Bednarz B, Caracappa PF, Xu XG. The development, validation and application of a multi-detector CT (MDCT) scanner model for assessing organ doses to the pregnant patient and fetus using Monte Carlo simulations. Phys Med Biol 2009;54:2699-2717.

Gudjonsdottir J, Svensson JR, Campling S, Brennan PC, Jonsdottir B. Efficient use of automatic exposure control systems in computed tomography requires correct patient positioning. Acta Radiol 2009; 50:1035-1041.

Habibzadeh MA, Ay MR, Asl AR, Gharidi H, Zaidi H. Impact of miscentering on patient dose and image noise in X-ray CT imaging: Phantom and clinical studies. Phys Med 2012; 28:191-199.

Hart D, Wall BF. UK population dose from medical X-ray examinations. Eur. Radiol. 2004;50:285-291.

Heaney DE, Norvill AJ. A Comparison of reduction in CT dose through the use of gantry angulations or bismuth shields. Australas Phys Eng Sci Med 2006;29:172-178.

Helasvuo T (ed.) Number of radiological examinations in Finland in 2011. STUK-B 161. Radiation and Nuclear Safety Authority, Helsinki 2013. (In Finnish)

Helmrot E, Pettersson H, Sandborg M, Nilssoin Altén J. Estimation of dose to the unborn child at diagnostic X-ray examinations based on data registered in RIS/PACS. Eur Radiol 2007;17:205-209.

Hérin E, Gardavaud F, Chiaradia M, Beaussart P, Richard P, Cavet M, Deux JF, Haioun C, Itti E, Rahmouni A, Luciani A. Use of model-based iterative reconstruction (MBIR) in reduced-dose CT for routine follow-up of patients with malignant lymphoma: dose savings, image quality and phantom study. Eur Radiol 2015;25:2362-2370.

Hopper KD, Neuman JD, King SH, Kunselman AR. Radioprotection to the eye during CT scanning. AJNR 2001;22:1194-1198.

Hubbell JH, Seltzer SM. Tables of x-ray mass attenuation coefficients and mass energy-absorption coefficients. National Institute of Standards and Technology (NIST), Gaithersburg, MD: NIST 2004.
http://physics.nist.gov/xaamdi

Huda W, Vance A. Patient radiation doses from adult and pediatric CT. AJR 2007;188:540-546.

Hugget J, Mukonoweshuro W, Loader R. A phantom-based evaluation of three commercially available patient organ shields for computed tomography X-ray examinations in diagnostic radiology. Radiat Prot Dosimetry 2013;155:161-168.

International Atomic Energy Agency (IAEA). Radiation oncology physics: a handbook for teachers and students. Vienna: IAEA 2005.

International Atomic Energy Agency (IAEA). Dosimetry in diagnostic radiology: an internation code of practice. Technical Reports series no. 457. Vienna: IAEA 2007.

International Atomic Energy Agency (IAEA). Diagnostic radiology physics: a handbook for teachers and students. Vienna: IAEA 2014.

International Commission on Radiological Protection (ICRP). 1990 Recommendations of the International Commission on Radiological Protection. ICRP Publication 60. Ann ICRP 1991;21:1-201.

International Commission on Radiological Protection (ICRP). Recommendations of the International Commission on Radiological Protection. ICRP Publication 103. Ann ICRP 2007;37(2-4):1-332.

International Commission on Radiation Units and Measurements (ICRU). Patient dosimetry for X-rays used in medical imaging. Report No. 74. Journal of the ICRU 2005;5(2):1-113.

International Electrotechnical Commission (IEC). Medical diagnostic X-ray equipment – radiation conditions for use in the determination of characteristics. IEC 61267, Geneva: IEC 2005.

Jaffe TA, Yoshizumi TT, Toncheva GI, Nguyen G, Hurwitz LM, Nelson RC. Early first-trimester fetal radiation dose estimation in 16-MDCT without and with automated tube current modulation. AJR 2008;190:860-864.

Jaffurs D, Denny A. Diagnostic pediatric computed tomographic scans of the head: Actual dosage versus estimated risk. Plast Reconstr Surg 2009;124:1254-1260.

Järvinen H, Seuri R, Kortesniemi M, Lajunen A, Hallinen E, Savikurki-Heikkilä P, Laarne P, Perhomaa M, Tyrväinen E. Indication-based national diagnostic reference levels for paediatric CT: a new approach with proposed values. Radiat Prot Dosimetry 2015;165:86-90.

Kalender WA, Wolf H, Suess C. Dose reduction in CT by anatomically adapted tube current modulation. II. Phantom measurements. Med Phys 1999;26:2248-2253.

Kalender WA, Buchenau S, Deak P, Kellermeier M, Langner O, van Straten M, Vollmar S, Wilharm S. Technical approaches to the optimisation of CT. Phys Med 2008;24:71-79.

Kalra MK, Maher MM, Toth TL, Hamberg LM, Blake MA, Shepard JA, Saini S. Strategies for CT radiation dose optimization. Radiology 2004a;230:619-628.

Kalra MK, Maher MM, Toth TL, Schimidt B, Westerman BL, Morgan HT, Saini S. Techniques and applications of automatic tube current modulation for CT. Radiology 2004b;233:649-657.

Katsura M, Matsuda I, Akahane M, Sato J, Akai H, Yasaka K, Kunimatsu A, Ohtomo K. Model-based iterative reconstruction technique for radiation dose reduction in chest CT: comparison with the adaptive statistical iterative reconstruction technique. Eur Radiol 2012;22:1613-1623.

Knoll GF. Radiation detection and measurement - 3rd ed. Hoboken, NJ: John Wiley & Sons, Inc. 2000.

Koivisto J, Kiljunen T, Tapiovaara M, Wolff J, Kortesniemi M. Assessment of radiation exposure in dental cone-beam computerized tomography with the use of metal-oxide semiconductor field-effect transistor (MOSFET) dosimeters and Monte Carlo simulations. Oral Surg Oral Med Oral Pathol Oral Radiol 2012;114:393-400.

Koivisto J, Kiljunen T, Wolff J, Kortesniemi M. Assessment of effective radiation dose of an extremity CBCT, MSCT and conventional X ray for knee area using MOSFET dosemeters. Radit Prot Dosimetry 2013a;157:515-524.

Koivisto J, Kiljunen T, Wolff J, Kortesniemi M. Characterization of MOSFET dosimeter angular dependence in three rotational axes measured free-in-air and in soft-tissue equivalent material. J Radiat Research 2013b;54:943-949.

Koivisto J, Wolf J, Kiljunen T, Schulze D, Kortesniemi M. Characterization of MOSFET dosimeters for low-dose measurements in maxillofacial anthropomorphic phantoms. J Appl Clinical Med Physics 2015;16:266-278.

Lee SJ, Park SH, Kim AY, Yang SK, Yun SC, Lee SS, Jung GS, Ha HK. A prospective comparison of standard-dose CT enterography and 50% reduced-dose CT enterography with and without noise reduction for evaluation Crohn disease. AJR 2011;197:50-57.

Lee C, Kim KP, Long DJ, Bolch WE. Organ doses for reference pediatric and adolescent patients undergoing computed tomography estimated by Monte Carlo simulation. Med Phys 2012;39:2129-2146.

Li J, Udayasankar UK, Toth TL, Seamans J, Small WC, Kalra MK. Automatic patient centering for MDCT: Effect on radiation dose. AJR 2007; 188:547-552.

Likert R. A technique for the measurement of attitudes. Archives of Psychology 1932;140:1-55.

Manninen AL. Clinical applications of radiophotoluminescence (RPL) dosimetry in evaluation of patient radiation exposure in radiology. Determination of absorbed and effective dose. Acta Univ Oul D. 1265. University of Oulu; 2014a. http://urn.fi/urn:isbn:9789526206240.

Manninen AL, Ojala K, Nieminen M, Perälä J. Fetal radiation dose in prophylatic uterine arterial embolization. Cardiovasc Intervent Radiol 2014b;37:942-948.

Martin CJ. Effective dose: how should it be applied to medical exposures? BJR 2007;80:639-647.

Matsubara K, Koshida K, Ichikawa K, Suzuki M, Takata T, Yamamoto T, Matsui O. Misoperation of CT automatic tube current modulation systems with inappropriate patient centering: Phantom studies. AJR 2009; 192:862-865.

Matsuoka S, Hunsaker AR, Gill RR, Oliva IB, Trotman-Dickenson B, Jacobson FL, Hatabu H. Vascular enhancement and image quality of MDCT pulmonary angiography in 400 cases: comparison of standard and low kilovoltage settings. AJR 2009;192:1651-1656.

McCollough CH, Leng S, Yu L, Cody DD, Boone JM, McNitt-Gray MF. CT dose index and patient dose: they are not the same thing. Radiology 2011;259:311-316.

McLaughlin DJ, Mooney RB. Dose reduction to radiosensitive tissues in CT. Do commercially available shields meet the users´s needs? Clinical Radiology 2004;59:446-450.

Mettler FA Jr, Huda W, Yoshizumi TT, Manesh M. Effective doses in radiology and diagnostic nuclear medicine: a catalog. Radiology 2008;248;254-263.

Miéville FA, Berteloot L, Grandjean A, Ayestaran P, Gudinchet F, Schmidt S, Brunelle F, Bochud FO, Verdun FR. Model-based iterative reconstruction in pediatric chest CT: assessment of image quality in a prospective study of children with cystic fibrosis. Pediatr Radiol 2013;43:558-567.

Muikku M, Bly R, Kurttio P, Lahtinen J, Lehtinen M, Siiskonen T, Turtiainen T, Valmari T, Vesterbacka K. The mean effective dose for Finns – Review 2012.

STUK-A 259. Radiation and Nuclear Safety Authority, Helsinki 2014. (In Finnish)

Nagel HD (ed.), Galanski M, Hidajat N, Maier W, Schmidt Th. Radiation exposure in computed tomography, 4th edition. Hamburg: CTB Publication, 2002.

National Council on Radiation Protection and Measurements (NCRP). Ionizing radiation exposure of the population of the United States. Report no. 160. Bethesda, MD: NCRP 2009.

Nievelstein RAJ, van Dam IM, van der Molen AJ. Multidetector CT in children: current concepts and dose reduction strategies. Pediatr Radiol 2010;40:1324-1344.

Norris H, Zhang Y, Bond J, Sturgeon GM, Minhas A, Tward DJ, Ratnanather JT, Miller MI, Frush D, Samei E, Segars WP. A set of 4D pediatric XCAT reference phantoms for multimodality research. Med Phys 2014;41:033701.

Padole A, Khawaja RDA, Kalra MK, Singh S. CT radiation dose and iterative reconstruction techniques. AJR 2015a;204:W384-W392.

Padole A, Singh S, Lira D, Blake MA, Pourjabbar S, Khawaja RDA, Choy G, Saini S, Do S, Kalra MK. Assessment of filtered back projection, adaptive statistical, and model-based iterative reconstruction for reduced dose abdominal computed tomography. J Comput Assist Tomogr 2015b;39:462-467.

Paterson A, Frush DP. Dose reduction in paediatric MDCT: general principles. Clin Radiol 2007;62:507-517.

Pearce MS, Salotti JA, Little MP, McHugh K, Lee C, Kim KP, Howe NL, Ronckers CM, Rajaraman P, Sir Craft AW, Parker L, Berrington de González A. Radiation exposure from CT scans in childhood and subsequent risk of leukaemia and brain tumours: a retrospective cohort study. Lancet 2012;380:499-505.

Peet DJ, Pryor MD. Evaluation of a MOSFET radiation sensor for the measurement of entrance surface dose in diagnostic radiology. BJR 1999;72:562-568.

Pickhardt PJ, Lubner MG, Kim DH, Tang J, Ruma JA, Muñoz del Rio A, Chen GH. Abdominal CT with model-based iterative reconstruction (MBIR): initial results of a prospective trial comparing ultralow-dose with standard-dose imaging. AJR 2012;199:1266-1274.

Pomije BD, Huh CH, Tressler MA, Hinterlang DE, Bolch WE. Comparison of angular free-in-air and tissue-equivalent phantom response measurements in p-MOSFET dosimeters. Health Phys 2001;80:497-505.

Preston DL, Ron E, Tokuoka S, Funamoto S, Nishi N, Soda M, Mabuchi K, Kodama K. Solid cancer incidence in atomic bomb survivors: 1958-1998. Radiat Res 2007;168:1-64.

Reimann AJ, Davison C, Bjarnason T, Thakur Y, Kryzmyk K, Mayo J, Nicolaou S. Organ-based computed tomographic (CT) radiation dose reduction to the lenses: impact on image quality for CT of the head. Comput Assist Tomogr 2012;36:334-338.

Rogers DWO. Fifty years of Monte Carlo simulations for medical physics. Phys Med Biol 2006;51:287-301.

Roschau JN, Hinterlang DE. Characterization of the angular response of an “Isotropic” MOSFET dosimeter. Health Phys 2003;84:376-379.

Samei E, Richard S. Assessment of the dose reduction potential of a model-based iterative reconstruction algorithm using a task-based performance metrology. Med Phys 2015;42:314-323.

Schindera ST, Winklehner A, Goetti R, Fischer M, Gnannt R, Szucs-Farkas Z. Effect of automatic tube voltage selection on image quality and radiation dose in abdominal CT angiography of various body sizes: a phantom study. Clin Radiol 2013;68:e79-86.

Schmidt B, Saltybaeva N, Kolditz D, Kalender WA. Assessment of patient dose from CT localizer radiographs. Med Phys 2013;40:084301.

Schueller-Weidekamm C, Schaefer-Prokop CM, Weber M, Herold CJ, Prokop M. CT angiography of pulmonary arteries to detect pulmonary embolism: Improvement of vascular enhancement with low kilovoltage settings. Radiology 2006;241:899-907.

Segars WP, Sturgeon G, Mendonca S, Grimes J, Tsui BM. 4D XCAT phantom for multimodality imaging research. Med Phys 2010;37:4902-4915.

Segars WP, Bond J, Frush J, Hon S, Eckersley C, Williams CH, Feng J, Tward DJ, Ratnanather JT, Miller MI, Frush D, Samei E. Population of anatomically variable 4D XCAT adult phantoms for imaging research and optimization. Med Phys 2013;40:043701.

Sigal-Cinqualbre AB, Hennequin R, Abada HT, Chen X, Paul JF. Low-kilovoltage multi-detector row chest CT in adults: Feasibility and effect on image quality and iodine dose. Radiology 2004;231:169-174.

Smith EA, Dillman JR, Goodsitt MM, Christodoulou EG, Keshavarzi N, Strouse PJ. Model-based iterative reconstruction: effect on patient radiation dose and image quality in pediatric body CT. Radiology 2014;270:526-534.

Sookpeng S, Martin CJ, Gentle DJ, Lopez-Gonzales MR. Relationship between patient size, dose and image noise under automatic tube current modulation systems. J Radiat Prot 2014;34:103.

Soubra M, Cygler J, Mackay GF. Evaluation of a dual bias dual metal oxide-silicon semiconductor field effect transistor detector as radiation dosimeter. Med Phys 1994;21:567-572.

STUK - Radiation and Nuclear Safety Authority. X-ray examinations in healthcare. Guide ST 3.3. Radiation and Nuclear Safety Authority, Helsinki 2006.

STUK - Radiation and Nuclear Safety Authority. Terveydenhuollon röntgenlaitteiden laadunvalvontaopas. STUK-tiedottaa 2/2008. (Guide for quality assurance of X-ray devices in healthcare. STUK Bulletin 2/2008 (In Finnish)). Helsinki: STUK 2008.

STUK - Radiation and Nuclear Safety Authority. Guidelines for paediatric CT examinations. Advice from STUK / September 2012. Radiation and Nuclear Safety Authority, Helsinki 2012.

Suzuki S, Furui S, Ishitake T, Abe T, Machida H, Takei R, Ibukuro K, Watanabe A, Kidouchi T, Nakano Y. Lens exposure during Brain scans using multidetector row CT scanners: methods for estimation lens dose. AJNR 2010;31:822-826.

Tan JSP, Tan KL, Lee JC, Wan CM, Leong JL, Chan LL. Comparison of eye lens dose on neuroimaging protocols between 16- and 64-section multidetector CT: achieving the lowest possible dose. AJNR 2009;30:373-377.

Taylor S, Litmanovich DE, Shahrzad M, Bankier AA, Genevois PA, Tack D. Organ-based tube current modulation: are women's breasts positioned in the reduced-dose zone? Radiology 2015;274:260-266.

Tenkanen-Rautakoski P (2008). Number of radiological examinations in Finland in 2005. STUK-B-STO 62. Radiation and Nuclear Safety Authority, Helsinki 2008. (In Finnish)

Thibault JB, Sauer KD, Bouman CA, Hsieh J. A three-dimensional statistical approach to improve image quality for multislice helical CT. Med Phys 2007;34:4526-4544.

Tian X, Li X, Segars WP, Paulson EK, Frush DP, Samei E. Pediatric chest and abdominopelvic CT: Organ dose estimation based on 42 patient models. Radiology 2014;270:535-547.

Tian X, Li X, Segars WP, Frush DP, Samei E. Prospective estimation of organ dose in CT under tube current modulation. Med Phys 2015;42:1575-1585.

Toth TL. Dose reduction opportunities for CT scanners. Pediatr Radiol 2002; 32:261-267.

Toth T, Ge Z, Daly MP. The influence of patient centering on CT dose and image noise. Med Phys 2007; 34:3093-3101.

Udayasankar UK, Li J, Baumgarten DA, Small WC, Kalra MK. Acute abdominal pain: value of non-contrast enhanced ultra-low-dose multi-detector row CT as a substitute for abdominal radiographs. Emerg Radiol 2009;16:61-70.

Vazquez JL, Pombar MA, Pumar JM, del Campo VM. Optimised low-dose multidetector CT protocol for children with cranial deformity. Eur Radiol 2013;23:2279-2287.

Wang J, Duan X, Christner JA, Leng S, Yu L, McCollough CH. Radiation dose reduction to the breast in thoracic CT: Comparison of bismuth shielding, organ-based tube current modulation, and use of a globally decreased tube current. Med Phys 2011;38:6084-6092.

Wang J, Duan X, Christner J, Leng S, Grant KL, McCollough GH. Bismuth shielding, organ-based tube current modulation, and global reduction of tube current for dose reduction to the eye at head CT. Radiology 2012a;262:191-198.

Wang J, Duan X, Christner JA, Leng S, Yu L, McCollough CH. Attenuation-based estimation of patient size for the purpose of size specific dose estimation in CT. Part I. Development and validation of methods using the CT image. Med Phys 2012b; 39:6764-6771.

Wang J, Christner JA, Duan X, Leng S, Yu L, McCollough CH. Attenuation-based estimation of patient size for the purpose of size specific dose estimation in CT. Part II. Implementation on abdomen and thorax phantoms using cross sectional CT images and scanned projection radiograph images. Med Phys 2012c; 39:6772-6778.

Widmann G, Schullian P, Gassner EM, Hoermann R, Bale R, Puelacher W. Ultralow-dose CT of the craniofacial bone for navigated surgery using adaptive statistical iterative reconstruction and model-based iterative reconstruction: 2D and 3D image quality. AJR 2015;204:563-569.

Winslow JF, Hyer DE, Fisher RF, Tien CJ, Hintenlang DE. Construction of anthropomorhic phantoms for use in dosimetry studies. J Appl Clinical Med Physics 2009;10:195-204.

Wintermark M, Lev MH. FDA investigates the safety of brain perfusion CT. AJNR 2010;31:2-3.

Yoshizumi TT, Goodman PC, Frush D, Nguyen G, Toncheva G, Sarder M, Barnes L. Validation of metal oxide semiconductor field effect transistor

technology for organ dose assessment during CT: comparison with thermoluminescent dosimetry. AJR 2007;188:1332-1336.

Yu L, Bruesewitz MR, Thomas KB, Fletcher JG, Kofler JM, McCollough CH. Optimal tube potential for radiation dose reduction in pediatric CT: principles, clinical implementations, and pitfalls. RadioGraphics 2011;31:835-848.

Zhang D, Li X, Gao Y, Xu G, Liu B. A method to acquire CT organ dose map using OSL dosimeters and ATOM anthropomorphic phantoms. Med Phys 2013;40:1-9.